MCB
Journals.ASM.org

Hepatic Mitogen-Activated Protein Kinase Phosphatase 1 Selectively Regulates Glucose Metabolism and Energy Homeostasis

Ahmed Lawan,[a] Lei Zhang,[a] Florian Gatzke,[a] Kisuk Min,[a] Michael J. Jurczak,[d,e] Mashael Al-Mutairi,[a] Patric Richter,[a] Joao Paulo G. Camporez,[d,e] Anthony Couvillon,[g] Dominik Pesta,[d,e] Rachel J. Roth Flach,[a]* Gerald I. Shulman,[d,e,f] Anton M. Bennett[a,b,c]

Departments of Pharmacology[a] and Comparative Medicine,[b] Yale University School of Medicine, New Haven, Connecticut, USA; Program in Integrative Cell Signaling and Neurobiology of Metabolism, Yale University School of Medicine, New Haven, Connecticut, USA[c]; Cellular & Molecular Physiology[d] and Internal Medicine, Section of Endocrinology and Metabolism,[e] Yale University School of Medicine, New Haven, Connecticut, USA; Howard Hughes Medical Institute, Yale School of Medicine, New Haven, Connecticut, USA[f]; Cell Signaling Technology Incorporated, Danvers, Massachusetts, USA[g]

The liver plays a critical role in glucose metabolism and communicates with peripheral tissues to maintain energy homeostasis. Obesity and insulin resistance are highly associated with nonalcoholic fatty liver disease (NAFLD). However, the precise molecular details of NAFLD remain incomplete. The p38 mitogen-activated protein kinase (MAPK) and c-Jun NH_2-terminal kinase (JNK) regulate liver metabolism. However, the physiological contribution of MAPK phosphatase 1 (MKP-1) as a nuclear antagonist of both p38 MAPK and JNK in the liver is unknown. Here we show that hepatic MKP-1 becomes overexpressed following high-fat feeding. Liver-specific deletion of MKP-1 enhances gluconeogenesis and causes hepatic insulin resistance in chow-fed mice while selectively conferring protection from hepatosteatosis upon high-fat feeding. Further, hepatic MKP-1 regulates both interleukin-6 (IL-6) and fibroblast growth factor 21 (FGF21). Mice lacking hepatic MKP-1 exhibit reduced circulating IL-6 and FGF21 levels that were associated with impaired skeletal muscle mitochondrial oxidation and susceptibility to diet-induced obesity. Hence, hepatic MKP-1 serves as a selective regulator of MAPK-dependent signals that contributes to the maintenance of glucose homeostasis and peripheral tissue energy balance. These results also demonstrate that hepatic MKP-1 overexpression in obesity is causally linked to the promotion of hepatosteatosis.

Obesity is a major problem globally, and its incidence is increasing at an alarming rate (1). Obesity predisposes to the development of nonalcoholic fatty liver disease (NAFLD), which is a spectrum of liver-related pathologies that encompasses steatosis, nonalcoholic steatosis, and nonalcoholic steatohepatitis (2). The development of hepatosteatosis arises as a result of an imbalance between triglyceride deposition and removal. Epidemiologically, NAFLD is associated with type 2 diabetes, suggesting that hepatosteatosis and the development of insulin resistance are causally linked (2). However, both genetic mouse models and clinical data suggest dissociation of hepatosteatosis from insulin resistance, arguing against the existence of such a causal link (3). Several proposed mechanisms have been put forth to explain the relationship between hepatosteatosis and insulin resistance. One mechanism proposes that type 2 diabetes results in hyperinsulinemia, which promotes hepatic lipogenesis and thus hepatosteatosis. Dysfunction in hepatic lipid metabolism and lipotoxicity have also been proposed to activate serine/threonine kinases that subsequently lead to the failure of insulin to signal (4).

The actions of kinases in physiological and pathophysiological metabolic pathways have been studied extensively (5, 6). In particular, the mitogen-activated protein kinase (MAPK) pathway is an established regulator of hepatic metabolism (7–10). The stress-responsive MAPK c-Jun NH_2-terminal kinase 1 (JNK1), when deleted specifically in the liver, results in the development of hepatosteatosis, enhanced hepatic glucose production, and insulin resistance (11). Additionally, p38 MAPK promotes gluconeogenesis through activation of the peroxisome proliferator-activated receptor γ coactivator 1α (PGC-1α) and through mediation of free fatty acid-induced p38 MAPK phosphorylation of the cyclic-AMP-responsive element binding protein (CREB) (9, 12). Collectively, these observations demonstrate an important role for the MAPKs in hepatic metabolism.

MAPK activity is opposed by specific dephosphorylation through the actions of MAPK phosphatases (MKPs) (13). The MKPs have been demonstrated to play a variety of roles in metabolic homeostasis (14). We have previously demonstrated that MKP-1, a nucleus-localized MKP, is a major negative regulator of p38 MAPK and JNK1/2 and functions to control metabolism (15). Whole-body deletion of MKP-1 in mice protects against diet-induced obesity (15, 16). Moreover, MKP-1-deficient mice fed a high-fat diet (HFD) (15) or mice in a genetic mouse model of obesity deficient for the expression of MKP-1 are protected from the development of hepatosteatosis (15, 17). These observations suggest that MKP-1 plays a crucial role in regulating liver metabolism. Mechanistically, MKP-1 functions to attenuate the ability of both p38 MAPK and JNK1/2 to phosphorylate and subse-

Received 16 April 2014 **Returned for modification** 30 May 2014
Accepted 3 October 2014

Accepted manuscript posted online 13 October 2014

Citation Lawan A, Zhang L, Gatzke F, Min K, Jurczak MJ, Al-Mutairi M, Richter P, Camporez JPG, Couvillon A, Pesta D, Roth Flach RJ, Shulman GI, Bennett AM. 2015. Hepatic mitogen-activated protein kinase phosphatase 1 selectively regulates glucose metabolism and energy homeostasis. Mol Cell Biol 35:26–40. doi:10.1128/MCB.00503-14.

Address correspondence to Anton M. Bennett, anton.bennett@yale.edu.

* Present address: Rachel J. Roth Flach, University of Massachusetts Medical School, Worcester, Massachusetts, USA.

doi:10.1128/MCB.00503-14

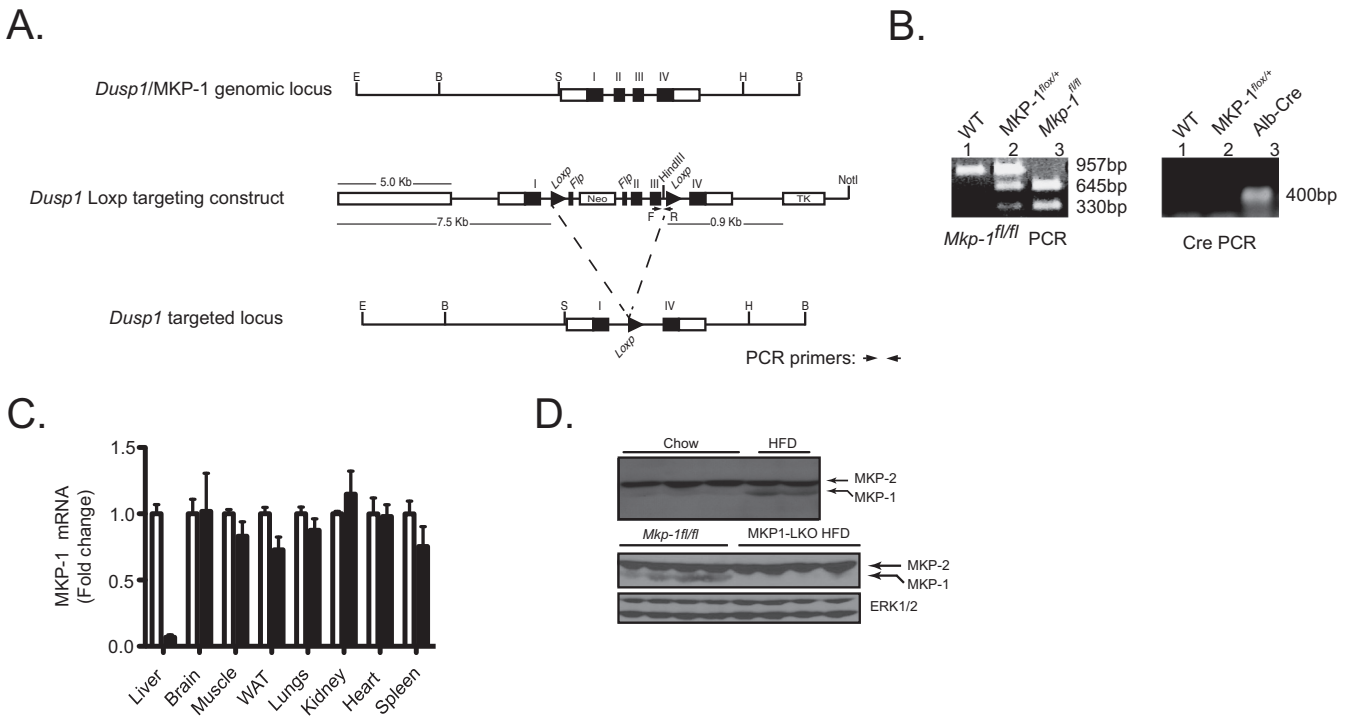

FIG 1 Generation and characterization of mice with liver-specific deletion of MKP-1. (A) Schematic of the *Dusp1*/MKP-1 gene locus, the targeted construct, and the resulting targeted allele. Cre-mediated excision results in the deletion of exons 2 and 3 of the Mkp-1 gene. The relevant restriction sites are indicated: B, BamHI; E, EcoRI; H, HindIII; S, ScaI. (B) *Mkp-1*$^{fl/fl}$ and MKP1-LKO genotyping by PCR using genomic DNA. (C) mRNA expression of MKP-1 from chow-fed *Mkp-1*$^{fl/fl}$ and MKP1-LKO mice ($n = 6$ to 10). Open bars, *Mkp-1*$^{fl/fl}$ mice; filled bars, MKP1-LKO mice. (D) Hepatic MKP-1 and MKP-2 protein expression from chow- and HFD-fed mice (upper panel) and *Mkp-1*$^{fl/fl}$ and MKP1-LKO mice fed an HFD (lower panel). ERK1/2 antibodies were used to detect the expression of ERK1/2 as a loading control.

quently activate transcription factors that are instrumental in the control of hepatic lipid metabolism (15, 17). MKP-1 regulates MAPK-mediated phosphorylation and activation of PPARα and PGC-1α (15, 16). MKP-1 also promotes lipogenesis by attenuating MAPK-dependent phosphorylation of PPARγ1 at the site, which negatively regulates the ability of PPARγ1 to engage in transcriptional activity (17). These results demonstrate an important role for MKP-1 in whole-body energy balance and also suggest that MKP-1 regulates MAPK-dependent pathways that control liver metabolism.

The goal of this study was to define the contribution of hepatic MKP-1 in the control of whole-body metabolism. To accomplish this, we generated mice specifically lacking the expression of MKP-1 in the liver, which represents the first tissue-specific deletion of an MKP family member. Our results show that MKP-1 is a critical regulator of hepatic lipid metabolism that integrates nuclear MAPK signaling in a manner that, when it is overexpressed in obesity, selectively promotes hepatosteatosis. Finally, an unanticipated connection between MKP-1 and the regulation of interleukin-6 (IL-6) and the liver hormone fibroblast growth factor 21 (FGF21) was uncovered, suggesting a role for hepatic MKP-1 in the systemic mediation of whole-body energy metabolism. Hence, hepatic MKP-1 represents a critical nodal point of MAPK regulation that links hepatic metabolic homeostasis to the control of whole-body metabolism.

MATERIALS AND METHODS

Reagents and antibodies. All reagents were purchased from standard chemical vendors. The following antibodies were used. Phospho-p38 MAPK (9215S), phospho-JNK1/2 (4668S), phospho-extracellular signal-regulated kinase 1/2 (phospho-ERK1/2) (9101S), phospho-STAT-3 (Y705) (9145S), phospho-STAT-3 (S727) (9134), phospho-CREB (S133) (9198S), phospho-α subunit of eukaryotic initiation factor 2 (phospho-eIF2α) (9721), STAT-3 (4904S), CREB (4820), JAK2 (3230), eIF2α (9722), and protein disulfide isomerase (PDI) (3501S) were obtained from Cell Signaling Technology. ERK1/2 (sc-94), p38 MAPK (sc-535), and JNK (sc-571) were obtained from Santa Cruz Biotechnology. GRP78 (AB53068) was obtained from Abcam. Antibodies to MKP-1 were generated using a chimeric peptide representing both the C terminus of MKP-1 and that of MKP-2 as an immunogen; these antibodies were obtained from Cell Signaling Technology.

Animal studies. The Yale University School of Medicine Institutional Animal Care and Use Committee approved all animal studies. Briefly, *loxP* sites flanking exons 2 and 3 of the *Dusp1*/MKP-1 gene locus were generated. A neomycin-selectable marker flanked by the *Flp* sites was placed downstream of the "floxed" exon 2 to allow for the removal of the neomycin cassette. Targeting was performed by standard techniques through the Yale Transgenics Core Facility. The targeting construct was introduced into 129Sv embryonic stem cells, and these cells were screened for neomycin resistance. Targeted cells were obtained and transfected with pOG-Flp-e6, which drives expression of the *Flpe* recombinase to obtain clones lacking the Neo cassette. PCR and Southern blotting identified clones in which the Neo resistance gene had been deleted and the genomic DNA with its appropriate modifications had been left intact. Embryonic stem (ES) cells in which the Neo cassette had been deleted were injected into mice, and mice chimeric for the mutation were crossed to C57BL/6 mice to generate F1 hybrids. F1 mice were backcrossed for 10 generations to a C57BL/6 background. MKP-1$^{flox/flox}$ (*Mkp-1*$^{fl/fl}$) mice were then bred with mice expressing the Cre recombinase under the control of an albumin promoter (Alb-Cre) to obtain Alb-Cre–MKP-1$^{flox/+}$

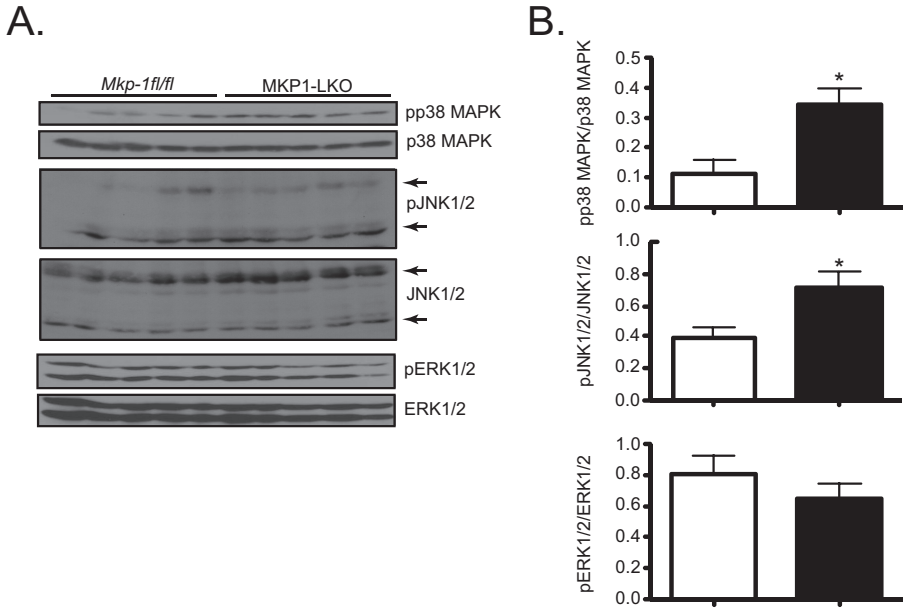

FIG 2 Enhanced hepatic MAPK phosphorylation in MKP1-LKO mice. (A) Liver lysates from chow-fed *Mkp-1*$^{fl/fl}$ and MKP1-LKO mice were analyzed by immunoblotting with the indicated antibodies. (B) Immunoblots were quantitated by densitometry for the levels of phospho-p38 MAPK/p38 MAPK, phospho-JNK1/2/JNK1/2, and phospho-ERK1/2/ERK1/2, as indicated. Results represent 10 to 13 mice per genotype, and data shown are the means ± SEM; ∗, $P < 0.05$, as determined by Student's *t* test. Open bars, *Mkp-1*$^{fl/fl}$ mice; filled bars, MKP1-LKO mice.

mice that were backcrossed to *Mkp-1*$^{fl/fl}$ mice to generate mice with liver-specific deletion of MKP-1, Alb-Cre–MKP-1$^{fl/fl}$, referred to as MKP-1 liver knockout (MKP1-LKO) mice. The Alb-Cre transgene was detected using primers specific to Alb-Cre and the MKP-1 "floxed" allele.

Metabolic measurements. Glucose tolerance tests (GTTs) were performed with 8- to 12-week-old male *Mkp-1*$^{fl/fl}$ and MKP-LKO littermates. Mice were fasted overnight for 16 h, followed by an intraperitoneal injection of glucose at 2 g/kg body weight. Blood glucose was measured by tail massaging at 0, 15, 30, 60, 90, and 120 min. Serum FGF21 levels was measured by using an enzyme-linked immunosorbent assay (ELISA) kit (Quantikine ELISA; R&D Systems), and leptin and IL-6 levels were determined by using a Milliplex map mouse serum adipokine kit (Millipore, MA). Hyperinsulinemic-euglycemic clamp studies were performed with male chow-fed *Mkp-1*$^{fl/fl}$ and MKP1-LKO mice at 12 weeks old at the Yale Metabolic Phenotyping Center. For the hyperinsulinemic-euglycemic clamp studies, catheters were implanted in these mice and they were allowed to recover 1 week prior to the clamp experiments. After an overnight 14-h fast, the mice were infused with [3-^{3}H]glucose at a rate of 0.05 μCi/min for 120 min to establish basal glucose turnover. The hyperinsulinemic-euglycemic clamp was performed with conscious mice for 140 min with a 4-min primed infusion (29 μU/kg) followed by a continuous (3 μU/kg/min) infusion of human insulin (Novolin; Novo Nordisk, Princeton, NJ), a continuous infusion of [3-^{3}H]glucose (0.1 μCi/min), and a variable infusion of 20% dextrose, given to maintain euglycemia. Blood samples were collected by tail massage for plasma glucose, insulin, and tracer levels at set time points during the 140-min infusion. The glucose turnover was calculated as the ratio of the [3-^{3}H]glucose infusion rate to the specific activity of plasma glucose at the end of the basal infusion and during the last 40 min of the hyperinsulinemic-euglycemic clamp experiment.

Conscious male *Mkp-1*$^{fl/fl}$ and MKP1-LKO mice were used to measure total body fat and lean mass using ^{1}H magnetic resonance spectroscopy (Bruker minispec analyzer; Echo Medical Systems, Houston, TX). Male chow-fed *Mkp-1*$^{fl/fl}$ and MKP1-LKO mice of ages between 8 and 12 weeks old were individually housed under controlled temperature (23°C) and lighting (12-h light, 12-h dark cycle; lights on at 0700 h) with free access to food and water. After 2 weeks of acclimatization, mice were kept in the metabolic cages (TSE Systems, Bad Homburg, Germany) for 1 week, and the food and water intake, energy expenditure, respiratory exchange ratio, and physical activity were assessed.

Isolation and culture of primary hepatocytes. Primary hepatocytes were isolated from 8- to 12-week-old male *Mkp-1*$^{fl/fl}$ and MKP1-LKO mice via portal cannulation. The liver was digested by perfusion with type IV collagenase (Worthington Biochemical Corp., Freehold, NJ) in Krebs-Ringer buffer (Sigma Chemical Co., St. Louis, MO). Dissociated cells were plated at 5×10^5 cells per well in rat tail type 1 collagen (Invitrogen, NY)-coated 6-well plates and allowed to adhere for 4 h in plating medium (Dulbecco's modified Eagle medium [DMEM]; Invitrogen, NY) containing 10% fetal bovine serum. Then, the plating medium was replaced with maintenance medium containing 0.2% bovine serum albumin (BSA), and cells were transfected with the promoter of FGF21 fused to luciferase for 48 h or stimulated with glucagon in the presence or absence of MAPK inhibitors.

Luciferase reporter assays. Primary hepatocytes were isolated from 8- to 12-week-old male *Mkp-1*$^{fl/fl}$ and MKP1-LKO mice and were transfected with the FGF21 promoter fused to luciferase (kindly provided by David Mangelsdorf, University of Southwestern Medical Center). Cells were transiently transfected with 500 ng of FGF21-luc and 10 ng renilla with Lipofectamine 2000. Cells were stimulated with 100 nM glucagon for 6 h or cells were incubated with 10 μM U0126, 10 μM SB203580, or 10 μM SP600125 for 1 h prior to stimulation with glucagon. HepG2 hepatoma cells were cotransfected with FGF21 luciferase promoter and either MKK6 (wild type [WT]) (13517; Addgene), MKK4 (WT) (14615; Addgene), or constitutively active mutants of the upstream activators of p38 MAPK, MKK6(EE) (13518; Addgene), JNK, and MKK4(EE) (14813; Addgene), or dominant negative mutants of p38 MAPK, MKK6(AA) (13519; Addgene), JNK, and MKK4(AA) (15314; Addgene). Also, HepG2 hepatoma cells were cotransfected with either pGL3-G6Pc or pGL-3-PCK1 promoter luciferase and MKK6(EE) and MKK7(DD) (16) in the presence or absence of pcDNA3.1-MKP-1. Plasmids were transfected with Lipofectamine 2000 (Invitrogen) according to the manufacturer's instructions. The activities of luciferase and renilla luciferase were assessed using

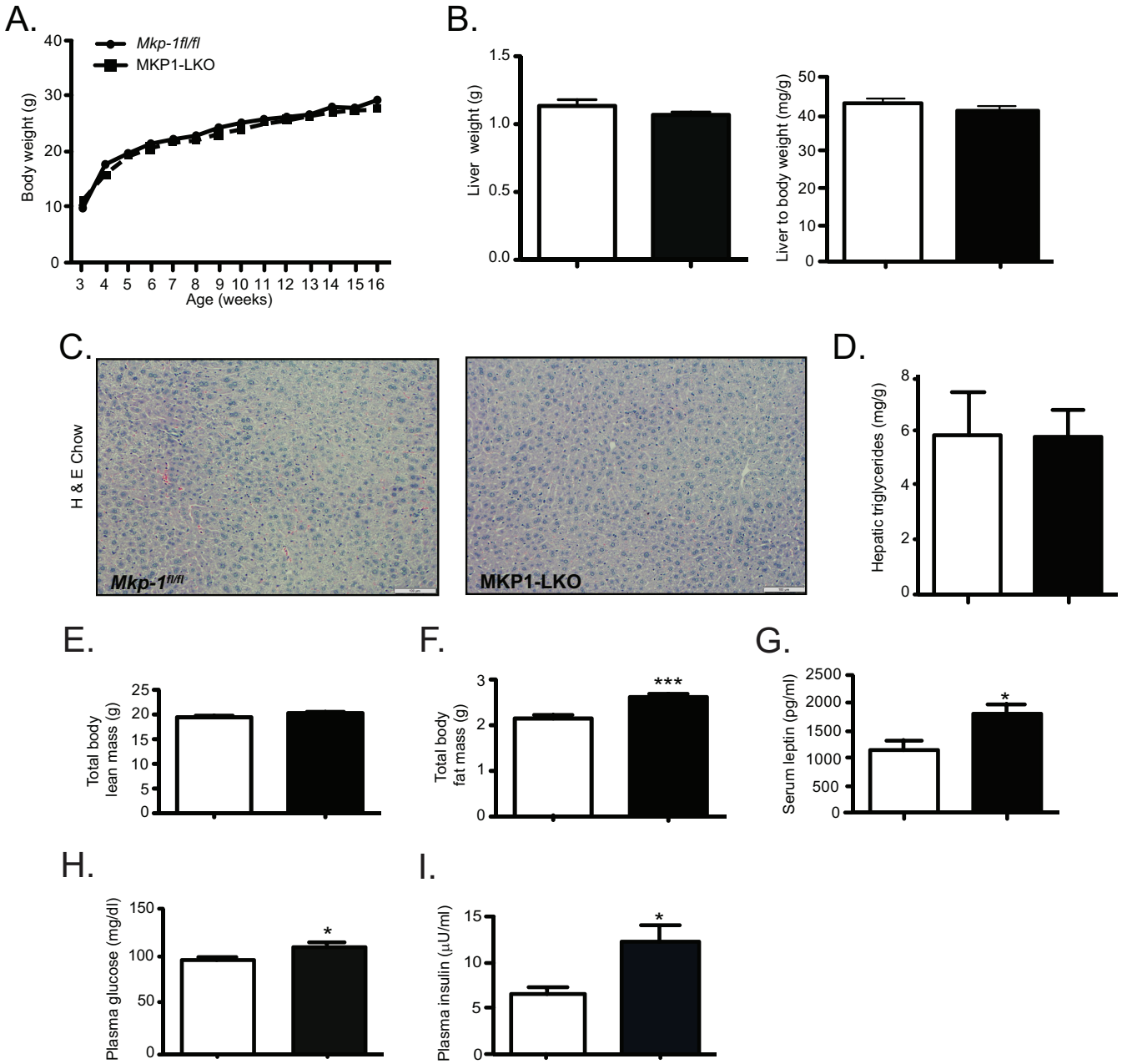

FIG 3 Increased adiposity, hyperglycemia, and hyperinsulinemia in chow-fed MKP1-LKO mice. (A) Weight curves of chow-fed male *Mkp-1*$^{fl/fl}$ and MKP1-LKO mice ($n = 10$ to 12 per genotype). (B) Liver weights and liver-to-body-weight ratio of chow-fed *Mkp-1*$^{fl/fl}$ and MKP1-LKO mice ($n = 10$ per genotype). (C and D) Representative hematoxylin-and-eosin staining of liver sections (C) and hepatic triglycerides from chow-fed *Mkp-1*$^{fl/fl}$ and MKP1-LKO mice ($n = 5$ to 8 for each genotype) (D). (E and F) Spectroscopic analysis of total body lean (E) and fat (F) mass of chow-fed *Mkp-1*$^{fl/fl}$ and MKP1-LKO mice ($n = 10$ per genotype). (G) Serum leptin in chow-fed *Mkp-1*$^{fl/fl}$ and MKP1-LKO mice ($n = 8$ per genotype). (H and I) Plasma glucose (H) and insulin (I) in chow-fed *Mkp-1*$^{fl/fl}$ and MKP1-LKO mice ($n = 15$ per genotype). Data represent the means ± SEM; ∗, $P < 0.05$; ∗∗∗, $P < 0.0001$ (as determined by Student's *t* test). Open bars, *Mkp-1*$^{fl/fl}$ mice; filled bars, MKP1-LKO mice.

the dual-luciferase reporter system kit from Promega (Madison, WI) according to the manufacturer's instructions, and luminescence was measured using a GloMax 20/20 luminometer (Promega Corporation, USA).

Histological analysis of tissue sections. Liver, skeletal muscle, and white adipose tissue were isolated from chow- and HFD-fed male *Mkp-1*$^{fl/fl}$ and MKP1-LKO mice and then fixed in 4% paraformaldehyde in phosphate-buffered saline (PBS), processed for paraffin sections, and stained with hematoxylin and eosin. Cryostat sections of livers were fixed with 4% paraformaldehyde-PBS for 1 h and cryoprotected with 20% sucrose prior to staining with 4% Oil Red O for 2 h. Liver tissues were fixed with 10% formalin in PBS for 2 h and then stained with 4% Oil Red O solution for 2 h.

Skeletal muscle mitochondrial oxygen consumption. Samples of muscle from chow- and HFD-fed male *Mkp-1*$^{fl/fl}$ and MKP1-LKO mice were placed in ice-cold buffer X containing 60 mM 2-(*N*-morpholino) ethanesulfonic acid (K-MES), 35 mM KCl, 7.23 mM K_2EGTA, 2.77 mM CaK_2EGTA, 20 mM imidazole, 0.5 mM dithiothreitol (DTT), 20 mM taurine, 5.7 mM ATP, 15 mM PCr, and 6.56 mM $MgCl_2$, pH 7.1. The

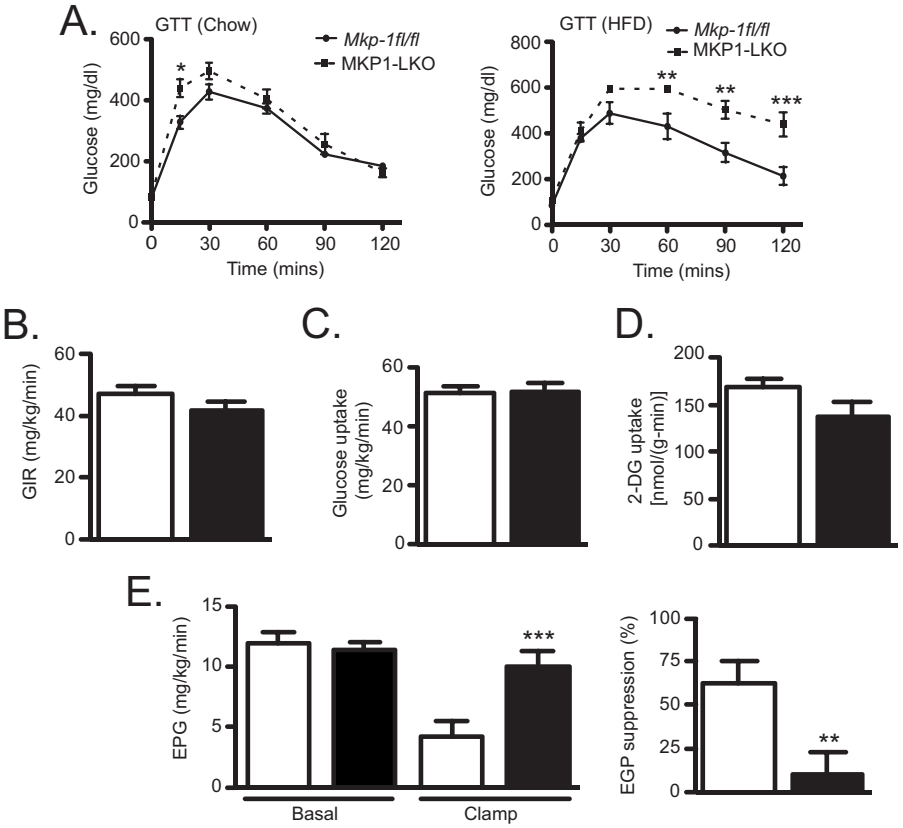

FIG 4 MKP1-LKO mice are glucose intolerant and exhibit hepatic insulin resistance. (A) Plasma glucose concentration during glucose tolerance tests in overnight fasted chow-fed (left panel) and HFD-fed (right panel) *Mkp-1*$^{fl/fl}$ and MKP1-LKO mice ($n = 15$ and $n = 8$ per genotype for chow- and HFD-fed mice, respectively). (B to E) Hyperinsulinemic-euglycemic clamps were performed on chow-fed *Mkp-1*$^{fl/fl}$ and MKP1-LKO mice, and the glucose infusion rate (GIR) (B), whole-body glucose uptake (C), skeletal muscle glucose uptake (D), and hepatic endogenous glucose production (EGP) and hepatic insulin action (E) were analyzed ($n = 10$ per genotype). Data are represented as means ± SEM; *, $P < 0.05$; **, $P < 0.01$; ***, $P < 0.0001$ (as determined by Student's *t* test and in panel A by analysis of variance [ANOVA] with Bonferroni's posttest for multiple comparisons). Open bars, *Mkp-1*$^{fl/fl}$ mice; filled bars, MKP1-LKO mice.

muscle was trimmed of connective tissue and fat. The muscle fiber bundles were gently separated in ice-cold buffer X to maximize the surface area of the fiber bundle. To permeabilize the myofibers, each fiber bundle was incubated in ice-cold buffer X containing 50 μg/ml saponin on a rotator for 30 min at 4°C. The permeabilized muscle bundles were then washed in ice-cold buffer Z containing 110 mM K-MES, 35 mM KCl, 1 mM EGTA, 5 mM K_2HPO_4, 3 mM $MgCl_2$, 0.005 mM glutamate, 0.02 mM malate, and 0.5 mg/ml BSA, pH 7.1.

Mitochondrial respiration was measured at 37°C in buffer Z using the Oroboros O2K oxygraph. After the respiration chamber was calibrated, permeabilized fiber bundles were incubated with 2 ml of respiration buffer Z containing 20 mM creatine to saturate creatine kinase. Flux through complex I was measured using 5 mM pyruvate and 2 mM malate. ADP-stimulated respiration (state 3) was measured by the addition of 500 μM ADP to the respiration chamber. Basal respiration (state 4) was determined in the presence of 10 μg/ml oligomycin to inhibit ATP synthesis. The respiratory control ratio (RCR) was calculated by dividing state 3 by state 4 respiration.

RNA extraction and real-time PCR analysis. RNA was isolated from either cells or tissues, including liver, skeletal muscle, white adipose tissue, brain, kidney, heart, lungs, and spleen, from male *Mkp-1*$^{fl/fl}$ and MKP1-LKO mice using an RNeasy kit (Qiagen, CA) according to the manufacturer's instructions. A total of 1 μg RNA was reverse transcribed to generate cDNA using a reverse transcriptase PCR kit (Applied Biosystems, CA). Real-time quantitative PCR was carried out in triplicate using the Applied Biosytems 7500 Fast real-time PCR system and TaqMan and SYBR green gene expression master mix with the following primer pairs: MKP-1, 5′-ATTTGCTGAACTCGGCACATTCGG-3′ and 3′-GGCAAGCGAAGAAACTGCCTCAAA-5′; PGC-1α, 5′-CCCTGCCATTGTTAAGACC-3′ and 3′-CTGCTGCTGTTCCTGTTTTC-5′; PCK1, 5′-CTAACTTGGCCATGATGAACC-3′ and 3′-CTTCACTGAGGTGCCAGGAG-5′; G6PC, 5′-TCGGAGACTGGTTCAACCTC-3′ and 3′-ACAGGTGACAGGGAACTGCT-5′; 18S rRNA, 5′-ACCGCAGCTAGGAATAATGGA-3′ and 3′-GCCTCAGTTCCGAAAACCA-5′; SREBP1c, 5′-ATCTCCTAGAGCGAGCGTTG and 3′-TATTTAGCAACTGCAGATATCCAAG; PPARγ, 5′-GTGCCAGTTTCGATCCGTAGA and 3′-GTAGGTGAAGAGAACGGCCTTGT. All relative gene expression levels were analyzed using the ΔC_T method and normalized to 18S rRNA expression. TaqMan primers and gene expression master mix from Applied Biosystems were used for POMC, neuropeptide Y (NPY), and AgRP mRNA quantitation.

Measurement of serum and hepatic lipids and glucose. Serum and hepatic triglyceride, ceramide, diacylglycerol, low-density lipoprotein (LDL), high-density lipoprotein (HDL), and long-chain acyl coenzyme A (LC-CoA) from 8- to 12-week-old fed male Mkp-1$^{fl/fl}$ and MKP-LKO mice were measured at the Yale Mouse Metabolic Phenotyping Center. Male chow-fed *Mkp-1*$^{fl/fl}$ and MKP1-LKO mice of ages between 8 and 12 week old were used for the measurement of plasma glucose concentrations by a glucose oxidase method using a Beckman glucose analyzer II. Measurement of plasma insulin was performed by using a radioimmunoassay kit (Linco Research, St. Louis, MO), and fatty acids were measured by a spectrophotometric technique (NEFA [nonesterified fatty acid] kit; Wako, Osaka, Japan).

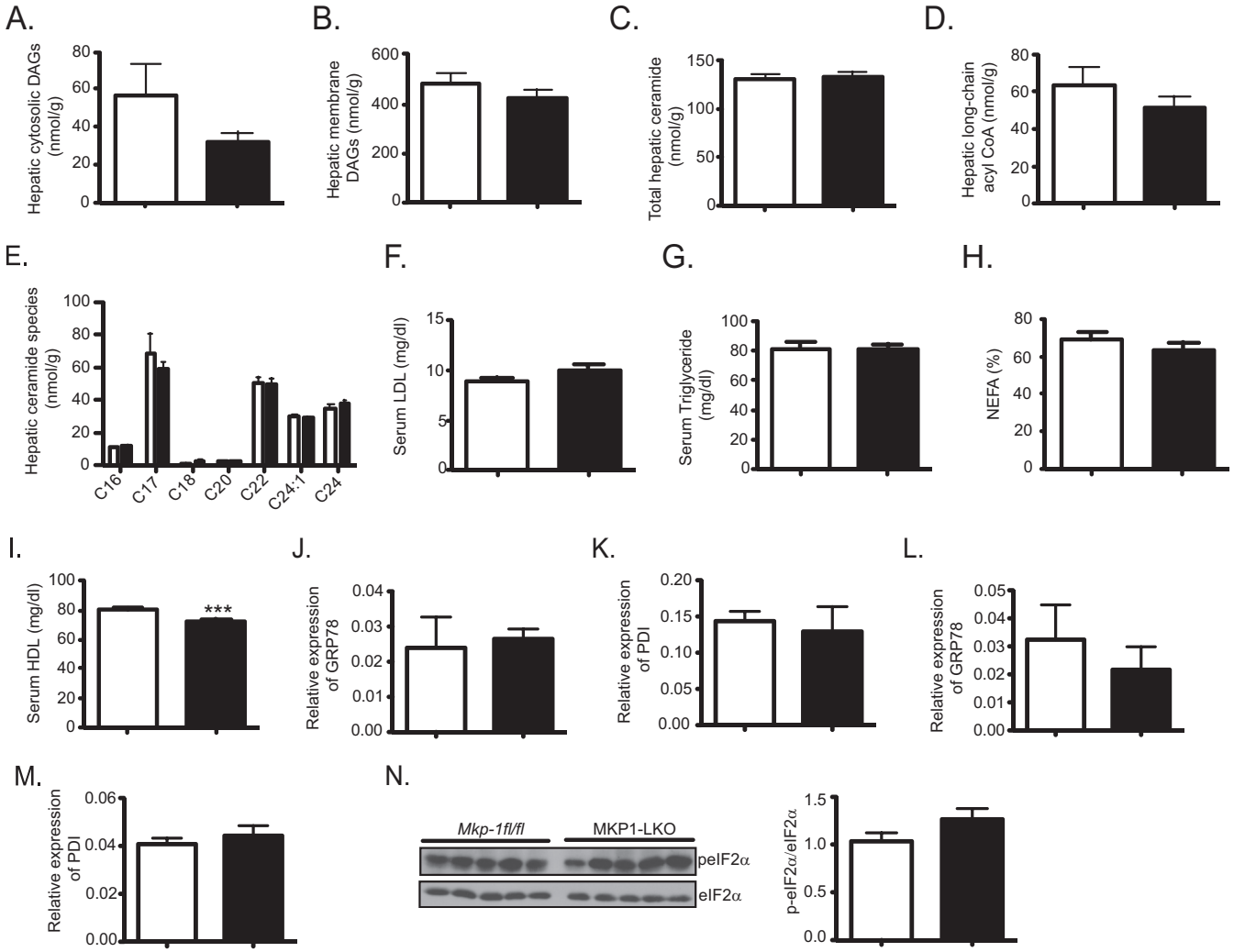

FIG 5 Hepatic and serum lipid profiles of chow-fed MKP1-LKO mice. (A to E) Hepatic cytosolic diacylglycerol (A), hepatic membrane diacylglycerol (B), total hepatic ceramide (C), hepatic long-chain acyl-CoA (D), and hepatic ceramide species (E) were measured for chow-fed *Mkp-1*$^{fl/fl}$ and MKP1-LKO mice ($n = 8$ per genotype). (F to I) Serum low-density lipoprotein (LDL) (F), serum triglycerides (G), serum nonesterified fatty acids (NEFA) (H), and serum high-density lipoprotein (HDL) (I) were measured for chow-fed *Mkp-1*$^{fl/fl}$ and MKP1-LKO mice ($n = 8$ per genotype). (J to N) Liver lysates from chow-fed (J and K) and HFD-fed (L, M, and N) *Mkp-1*$^{fl/fl}$ and MKP1-LKO mice were analyzed by immunoblotting using anti-GRP78, anti-PDI, phospho-eIF2α, and anti-eIF2α antibodies. Immunoblots were quantified by densitometry ($n = 4$ or 5 mice per genotype). Data represent means ± SEM; ***, $P < 0.0001$, as determined by Student's *t* test. Open bars, *Mkp-1*$^{fl/fl}$ mice; filled bars, MKP1-LKO mice.

Immunoblotting. Liver tissue was homogenized in RIPA buffer (25 mM Tris · HCl [pH 7.4], 150 mM NaCl, 5 mM EDTA, 1% NP-40, 0.1% SDS, and 1.0% sodium deoxycholic acid), supplemented with protease and phosphatase inhibitors (5 μg/ml leupeptin, 5 μg/ml aprotinin, 1 μg/ml pepstatin A, 1 mM phenylmethylsulfonyl fluoride [PMSF], 1 mM benzamidine, 1 mM Na_3VO_3, and 10 mM NaF). Homogenates were lysed for 30 min on the shaker at 4°C prior to clarification at 20,800 × *g* for 30 min at 4°C. Protein concentrations were determined by using a Pierce bicinchoninic acid (BCA) protein assay kit (Pierce, Rockford, IL). Lysates were resolved by SDS-PAGE and transferred to nitrocellulose membranes, which were incubated with phospho-specific antibodies, followed by enhanced chemiluminescence detection.

Statistical analysis. All data represent the means ± standard errors of the means (SEM). Differences between groups were assessed using a Student *t* test or analysis of variance (ANOVA) with Bonferroni's posttest for multiple comparisons using the GraphPad Prism 6 statistical software program.

RESULTS

Generation of liver-specific-MKP-1-deficient mice. Previous data using whole-body MKP-1-deficient mice suggested a metabolic role for MKP-1 in the liver (15, 17). To further define the contribution of MKP-1 in the liver, we generated MKP-1 liver-specific knockout mice (MKP1-LKO) using the Cre-*loxP* strategy. Mice containing a floxed allele between exons 2 and 3 of the *Dusp1*/MKP-1 locus were intercrossed with albumin-Cre-expressing mice to generate *Mkp-1*$^{fl/fl}$*–Alb-Cre* progeny (Fig. 1A and B). Quantitative PCR analysis of MKP-1 mRNA expression among several different tissues isolated from MKP1-LKO mice confirmed that MKP-1 was deleted specifically in the liver (Fig. 1C). In the livers of mice fed a chow diet, the protein expression of MKP-1 was low but detectable (Fig. 1D, upper panel). However, these basal levels of MKP-1 protein expression were dramatically

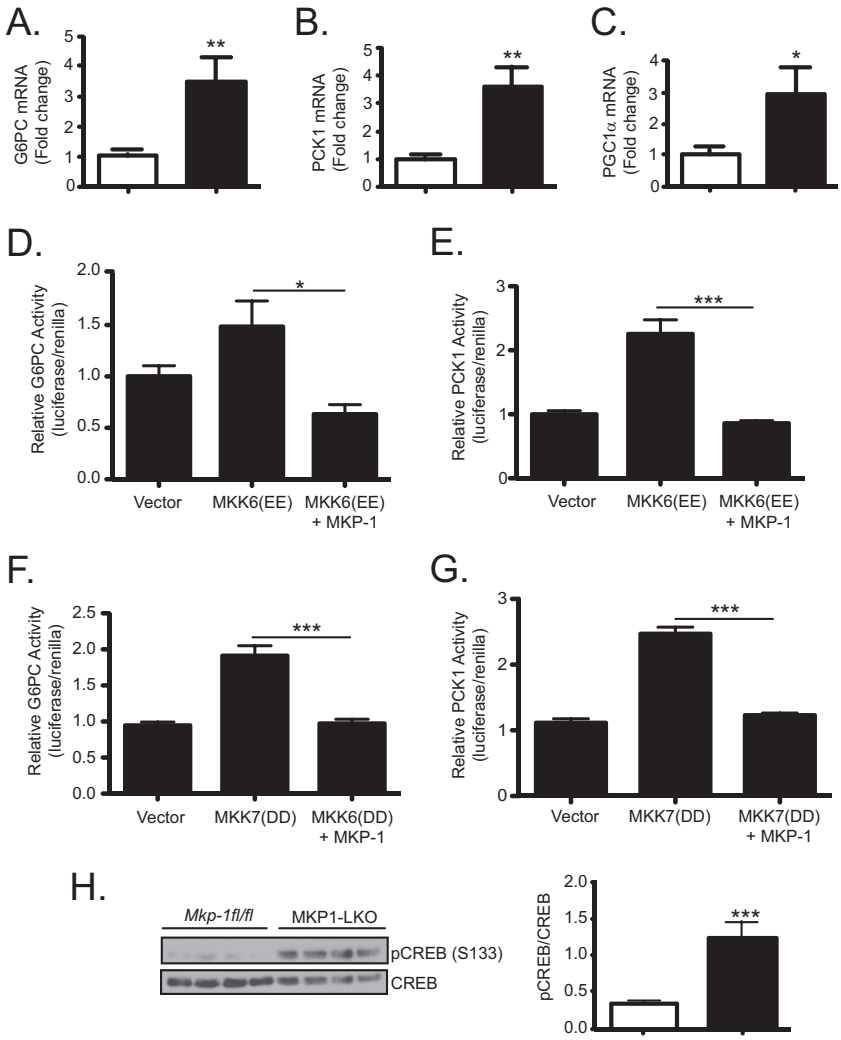

FIG 6 Regulation of gluconeogenic genes by hepatic MKP-1. (A to C) mRNA expression of *G6pc*, *Pck1*, and *Pgc1*α from livers of overnight-fasted chow-fed *Mkp-1*$^{fl/fl}$ and MKP1-LKO mice ($n = 10$ per genotype). Changes in relative luciferase activity in HepG2 hepatoma cells transfected with either pGL3-G6Pc or pGL-3-PCK1 promoter luciferase in the presence or absence of MKP-1 are shown. Constitutively active mutants of the upstream activators of p38 MAPK [MKK6(EE)] and JNK [MKK7(DD)] were overexpressed to induce p38 MAPK and JNK activity, respectively. (D to G) Glucose 6-phosphatase (G6Pase) (D and F) and phosphoenolpyruvate carboxykinase (PEPCK) (E and G). (H) Liver lysates from chow-fed *Mkp-1*$^{fl/fl}$ and MKP1-LKO mice were analyzed by immunoblotting using phospho-CREB (S133) and CREB antibodies ($n = 8$ to 10 per genotype). Data represent the means ± SEM; *, $P < 0.05$; **, $P < 0.01$; ***, $P < 0.0001$ (as determined by Student's *t* test and in panels D to G by analysis of variance [ANOVA] with Bonferroni's posttest for multiple comparisons). Open bars, *Mkp-1*$^{fl/fl}$ mice; filled bars, MKP1-LKO mice.

upregulated in HFD-fed *Mkp-1*$^{fl/fl}$ mice (Fig. 1D, upper panel). Importantly, in HFD-fed MKP1-LKO mice, the expression of MKP-1 was not detectable, confirming the deletion of the MKP-1 protein in the liver without discernible compensatory expression from the highly related MKP family member MKP-2 (Fig. 1D, lower panel). Consistent with the MKP-1 whole-body knockout phenotype (15), MKP1-LKO mice exhibited enhanced hepatic p38 MAPK and JNK1/2 but not ERK1/2 phosphorylation (Fig. 2A and B). Hence, the lack of hepatic MKP-1 expression results in the commensurate upregulation of both p38 MAPK and JNK phosphorylation, demonstrating that functional loss of MKP-1 has been achieved in this mouse model. These data also show that MKP-1 becomes upregulated in the liver in obese states.

Hepatic MKP-1 negatively regulates gluconeogenesis. MKP1-LKO mice showed body weight, liver weight, histology, and hepatic triglycerides comparable to those of *Mkp-1*$^{fl/fl}$ mice when fed a chow diet (Fig. 3A to D). MKP1-LKO mice also showed a level of lean mass equivalent to that of wild-type mice (Fig. 3E). However, unlike MKP-1 whole-body-deficient mice on a chow diet (15), MKP1-LKO mice showed increased levels of adiposity (Fig. 3F) which, correlated with significantly elevated serum leptin levels compared with those of *Mkp-1*$^{fl/fl}$ littermates (Fig. 3G). MKP1-LKO mice developed significant fasting hyperglycemia compared with *Mkp-1*$^{fl/fl}$ mice (Fig. 3H), and compensatory hyperinsulinemia on a chow diet was significant in MKP1-LKO mice (Fig. 3I). These results reveal that hepatic MKP-1 contributes to the maintenance of glucose homeostasis.

To examine whether hepatic MKP-1 regulates glucose homeostasis, we performed glucose tolerance tests. These results revealed that MKP1-LKO mice are modestly glucose intolerant in compar-

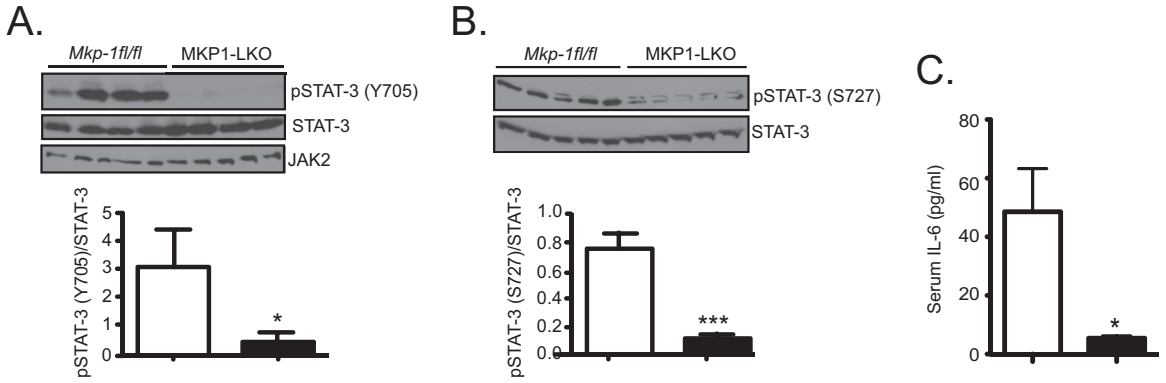

FIG 7 Impaired STAT-3 phosphorylation and IL-6 expression in MKP1-LKO mice. (A and B) Liver lysates from chow-fed *Mkp-1*$^{fl/fl}$ and MKP1-LKO mice were analyzed by immunoblotting with phospho-STAT-3 (Y705) (A) or phospho-STAT-3 (S727) (B); STAT-3 and JAK2 antibodies were used as controls ($n = 8$ to 10 per genotype). (C) Serum IL-6 in chow-fed *Mkp-1*$^{fl/fl}$ and MKP1-LKO mice. Data represent the means ± SEM; *, $P < 0.05$; ***, $P < 0.0001$ (as determined by Student's *t* test). Open bars, *Mkp-1*$^{fl/fl}$ mice; filled bars, MKP1-LKO mice.

ison with *Mkp-1*$^{fl/fl}$ mice under chow feeding conditions (Fig. 4A), but this was significantly exacerbated in HFD-fed MKP1-LKO mice (Fig. 4A). In order to assess insulin action and sensitivity in specific tissues, we performed hyperinsulinemic-euglycemic clamps in chow-fed MKP1-LKO and *Mkp-1*$^{fl/fl}$ mice. These studies showed no significant difference in the glucose infusion rate required to maintain euglycemia (Fig. 4B), and no difference in either whole-body (Fig. 4C) or skeletal muscle (Fig. 4D) glucose uptake were observed in MKP1-LKO mice compared with that for *Mkp-1*$^{fl/fl}$ littermates. However, clamped hepatic glucose production was significantly greater and suppression of hepatic glucose production by insulin was impaired by approximately 60%, indicating that MKP1-LKO mice exhibit hepatic insulin resistance (Fig. 4E). These data demonstrate that MKP1-LKO mice are hyperglycemic and glucose intolerant and develop hepatic insulin resistance.

Dysfunctional lipid metabolism and the unfolded protein response are implicated in the development of hepatic insulin resistance (4, 18). Analyses of hepatic lipid metabolites (Fig. 5A to E), serum lipids (Fig. 5F to I), and markers of the unfolded protein response (Fig. 5J to N) were unremarkable between MKP1-LKO and *Mkp-1*$^{fl/fl}$ mice, suggesting a lack of involvement of either lipotoxicity or endoplasmic reticulum stress in the development of hepatic insulin resistance in chow-fed MKP1-LKO mice.

It has been demonstrated that p38 MAPK promotes gluconeogenesis (9, 19) and enhanced gluconeogenic flux can facilitate the development of hepatic insulin resistance (20). Therefore, we analyzed the mRNA expression of glucose-6-phosphatase (*G6pc*) and phosphoenolpyruvate carboxykinase (*Pck1*). We found that expression of both genes was significantly increased in MKP1-LKO mice compared with that in *Mkp-1*$^{fl/fl}$ littermates (Fig. 6A and B). PGC-1α, which promotes gluconeogenesis (21), was significantly upregulated in MKP1-LKO mice compared with results for *Mkp-1*$^{fl/fl}$ mice (Fig. 6C). Next, we used constitutively active mutants of MKK6 and MKK7 in order to determine the effects of MKP-1 overexpression on p38 MAPK and JNK-mediated effects on *G6Pase* and *Pck1* gene expression. Both activated mutants of MKK6 and MKK7 stimulated the expression of G6Pase- and Pck1-mediated luciferase activity (Fig. 6D to G). Overexpression of MKP-1 inhibited p38 MAPK-mediated (Fig. 6D and E) and JNK-mediated (Fig. 6F and G) activation of *G6Pase* and *Pck1* transcriptional activity. These results establish MKP-1 as a negative regulator of gluconeogenesis by opposing both p38 MAPK- and JNK-mediated activation of *Pck1* and *G6pc*.

Next, we examined signaling components that are known to be critical regulators of the gluconeogenic pathway. First, we investigated the status of activation of the cAMP-responsive element binding protein (CREB), which promotes gluconeogenesis (22, 23). Consistent with our previous findings (24), phosphorylation of CREB, which is activated by Ser 133 phosphorylation, was significantly increased at this site in livers of MKP1-LKO mice (Fig. 6H). Collectively, these results demonstrate that hepatic MKP-1 is an essential negative regulator of gluconeogenesis by acting through a p38 MAPK-dependent pathway to suppress CREB phosphorylation.

We further explored the mechanism of MKP-1 regulation of gluconeogenesis by assessing the activity of the signal transducer and activator of transcription 3 (STAT-3), which negatively regulates gluconeogenesis, by inhibiting *G6pc* and *Pck1* (25). We found that in livers of MKP1-LKO mice, STAT-3 tyrosine 705 (Tyr-705) phosphorylation was significantly reduced compared with that of *Mkp-1*$^{fl/fl}$ mice (Fig. 7A). The expression levels of Janus kinase 2 (JAK2) and the upstream STAT-3 tyrosine kinase were comparable between the two genotypes (Fig. 7A). STAT-3 serine 727 (Ser-727) phosphorylation is also required for its transcriptional activation (26), and this site was reduced in phosphorylation in the livers of MKP1-LKO mice compared with results for *Mkp-1*$^{fl/fl}$ littermates (Fig. 7B). The apparent disruption of STAT-3 signaling in MKP1-LKO mice suggested the possibility that cytokines that signal through this pathway are altered in their levels of expression. Interleukin-6 (IL-6) is a potent metabolic cytokine that acts through the JAK/STAT pathway to suppress gluconeogenesis (27). We therefore, examined whether the circulating expression levels of IL-6 were reduced in MKP1-LKO mice. Remarkably, we found that MKP1-LKO mice exhibited dramatically reduced expression of circulating IL-6 levels compared with wild-type controls (Fig. 7C). These results reveal the surprising relationship between hepatic MKP-1 and the expression of IL-6. The loss of circulating IL-6 expression likely contributes to the impaired signaling to STAT-3 in MKP1-LKO mice and hence unabated gluconeogenic gene expression.

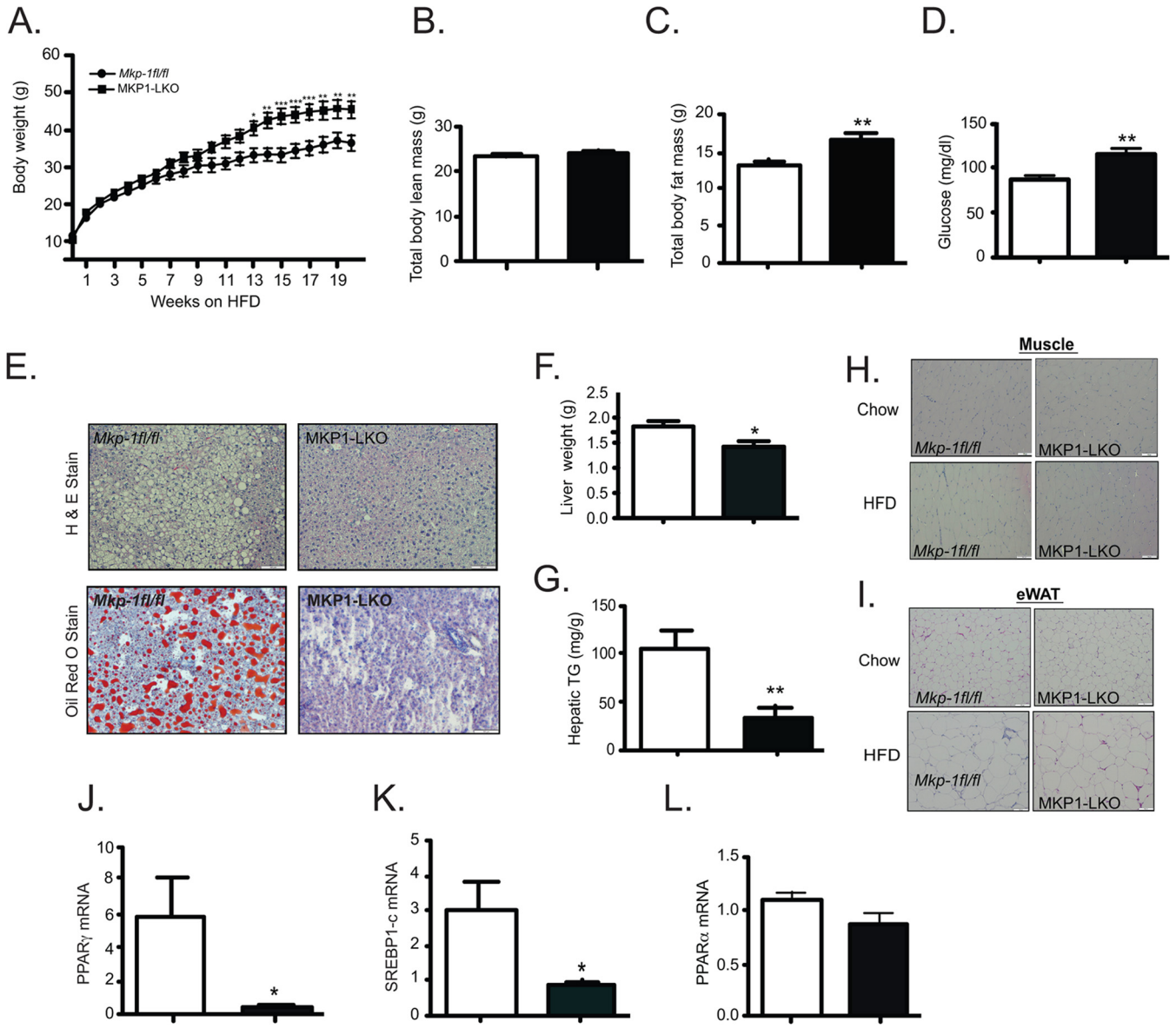

FIG 8 Susceptibility to diet-induced obesity and protection from hepatosteatosis in MKP1-LKO mice. (A) Weight curves of HFD-fed male *Mkp-1*$^{fl/fl}$ ($n = 9$) and MKP1-LKO ($n = 10$) mice for 20 to 24 weeks. (B and C) Spectroscopic analysis of total body lean mass (B) or total body fat mass (C) from HFD-fed *Mkp-1*$^{fl/fl}$ and MKP1-LKO mice ($n = 8$ per genotype). (D) Blood glucose values from HFD-fed *Mkp-1*$^{fl/fl}$ and MKP1-LKO mice ($n = 8$ per genotype). (E) Representative hematoxylin-and-eosin and Oil Red O staining of liver sections from HFD-fed *Mkp-1*$^{fl/fl}$ and MKP1-LKO mice. (F) Liver weights of HFD-fed *Mkp-1*$^{fl/fl}$ and MKP1-LKO mice ($n = 8$ per genotype). (G) Hepatic triglycerides (TG) from HFD-fed *Mkp-1*$^{fl/fl}$ and MKP1-LKO mice ($n = 8$ per genotype). (H) Representative hematoxylin-and-eosin staining of skeletal muscle sections from chow- and HFD-fed *Mkp-1*$^{fl/fl}$ and MKP1-LKO mice ($n = 5$ per genotype). (I) Representative hematoxylin-and-eosin staining of epididymal white adipose tissue (eWAT) sections from chow- and HFD-fed *Mkp-1*$^{fl/fl}$ and MKP1-LKO mice ($n = 5$ per genotype). (J to L) Hepatic mRNA expression of PPARγ (J), Srebp1c (K), or PPARα (L) from HFD-fed *Mkp-1*$^{fl/fl}$ and MKP1-LKO mice ($n = 8$ per genotype). Data represent means ± SEM; *, $P < 0.05$; **, $P < 0.01$; ***, $P < 0.0001$ (as determined by Student's *t* test or in panel A by analysis of variance [ANOVA] with Bonferroni's posttest for multiple comparisons). Open bars, *Mkp-1*$^{fl/fl}$ mice; filled bars, MKP1-LKO mice.

Loss of hepatic MKP-1 protects against hepatic steatosis. MKP-1 whole-body-deficient mice are protected from diet-induced obesity and the acquisition of hepatic steatosis (15–17). In contrast, MKP1-LKO mice when placed on a HFD were susceptible to diet-induced obesity compared with *Mkp-1*$^{fl/fl}$ controls (Fig. 8A). The increased weight gain in MKP1-LKO mice was largely attributable to an increase in adiposity rather than in lean mass (Fig. 8B and C). HFD-fed MKP1-LKO mice also exhibit significant fasting hyperglycemia (Fig. 8D). Since MKP1-LKO mice are sensitive to diet-induced obesity and succumb to hepatic insulin resistance, susceptibility to the development of hepatic steatosis was anticipated. Surprisingly, MKP1-LKO mice were protected from the development of hepatic steatosis when fed an HFD (Fig. 8E), consistent with the reduced liver weight and hepatic triglyceride accumulation (Fig. 8F and G). Skeletal muscle and white adipose tissue were histologically similar between MKP1-LKO and *Mkp-1*$^{fl/fl}$ controls (Fig. 8H and I). Consistent with the protection from fatty liver, the expression of mRNAs for PPARγ and

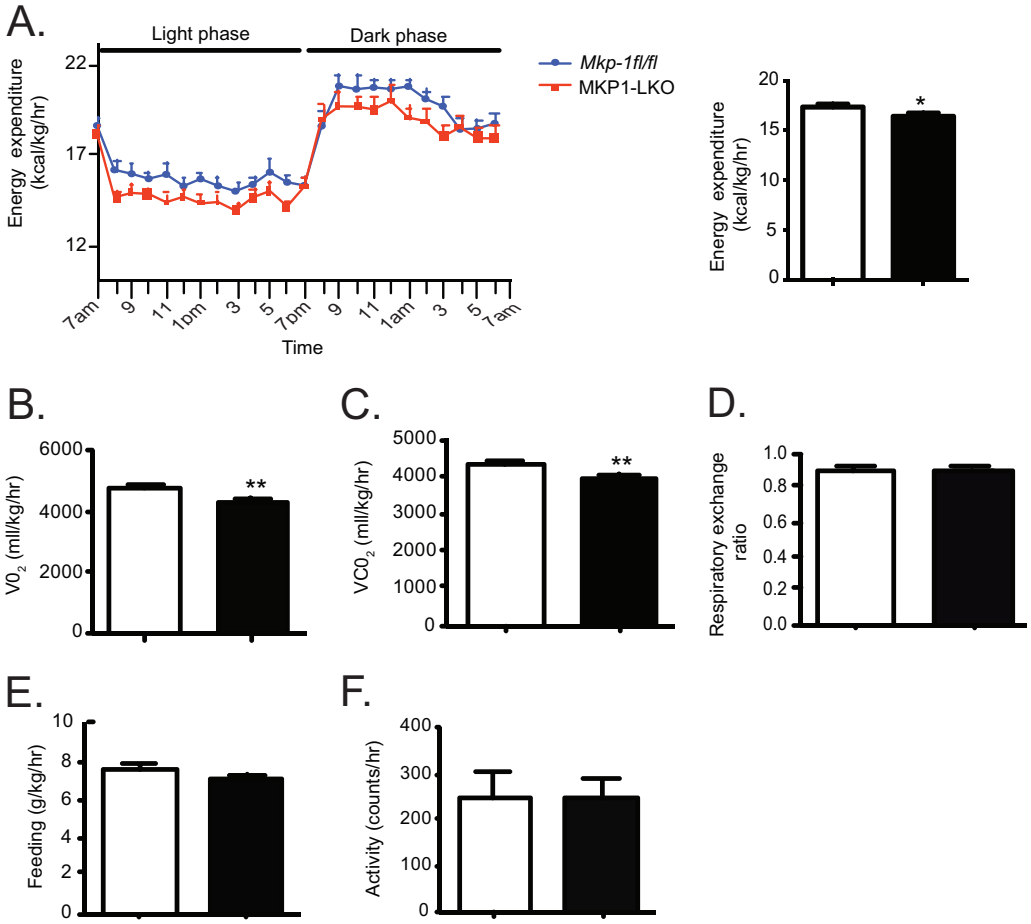

FIG 9 Reduced energy expenditure in MKP1-LKO mice. Chow-fed *Mkp-1*$^{fl/fl}$ and MKP1-LKO mice were subjected to open-circuit calorimetry. (A) Energy expenditure; (B) oxygen consumption; (C) carbon dioxide production; (D) respiratory exchange ratio; (E) feeding; (F) locomotor activity ($n = 8$ per genotype). Data represent means ± SEM; *, $P < 0.05$; **, $P < 0.01$ (as determined by Student's *t* test). Open bars, *Mkp-1*$^{fl/fl}$ mice; filled bars, MKP1-LKO mice.

sterol regulatory element-binding protein 1c (SREBP-1c) but not that of PPARα was significantly reduced in the livers of MKP1-LKO mice (Fig. 8J to L). These data suggest that MKP-1 upregulation in obesity (Fig. 1D) selectively promotes hepatic lipogenesis and is uncoupled under HFD conditions from participating in the maintenance of glucose homeostasis.

Reduced energy expenditure in hepatic MKP-1-deficient mice. In order to examine the basis for the sensitivity to weight gain in MKP1-LKO mice, we performed metabolic calorimetry. Chow-fed MKP1-LKO mice displayed significantly decreased energy expenditure levels and oxygen and carbon dioxide consumption compared with those of *Mkp-1*$^{fl/fl}$ littermates (Fig. 9A to C). No differences in respiratory exchange ratio, food intake, or activity between the two genotypes were observed (Fig. 9 to F). Previously, we observed that whole-body MKP-1 deficiency results in increased energy expenditure, consistent with the observed resistance to diet-induced obesity (15). Here, we found hepatic MKP-1 to be involved in promoting energy utilization, which is in line with the susceptibility of MKP1-LKO mice to gaining weight on a high-fat diet.

These results could reflect the decreased expression levels of circulating IL-6 (Fig. 7C). Studies have demonstrated that IL-6 exerts its metabolic effects centrally rather than by acting on peripheral sites (28). Therefore, we considered the possibility that hepatic MKP-1 was indirectly regulating IL-6 expression, which in turn was controlling energy expenditure by affecting hypothalamic neuropeptide expression. Therefore, we determined the expression levels of hypothalamic neuropeptides, neuropeptide Y (NPY), agouti-related peptide (AgRP), and propriomelanocortin (29) in MKP1-LKO mice. We found no observable changes in hypothalamic mRNA expression levels of NPY, AgRP, or propriomelanocortin in either chow- or HFD-fed MKP1-LKO mice (Fig. 10). Hence, consistent with a lack of effect on food intake, it is unlikely that decreases in energy expenditure in MKP1-LKO mice are associated with a central neuroendocrine effect. It is conceivable that the decreased levels of energy expenditure in MKP1-LKO mice arise either from intrinsic decreases in hepatic energy consumption and/or factors released by the liver that influence systemic whole-body energy balance. Given that the contribution of the liver toward whole-body energy expenditure is relatively minor, it is more likely that MKP1-LKO mice might have defects in the regulation of hepatokines that influence systemic energy metabolism.

Hepatic MKP-1 is required for the expression of FGF21. In order to evaluate the possibility that MKP-1 regulates the expression of hormones and/or cytokines that systemically regulate energy expenditure, we surveyed for differences between wild-type and MKP1-LKO mice for hepatically secreted hormones known

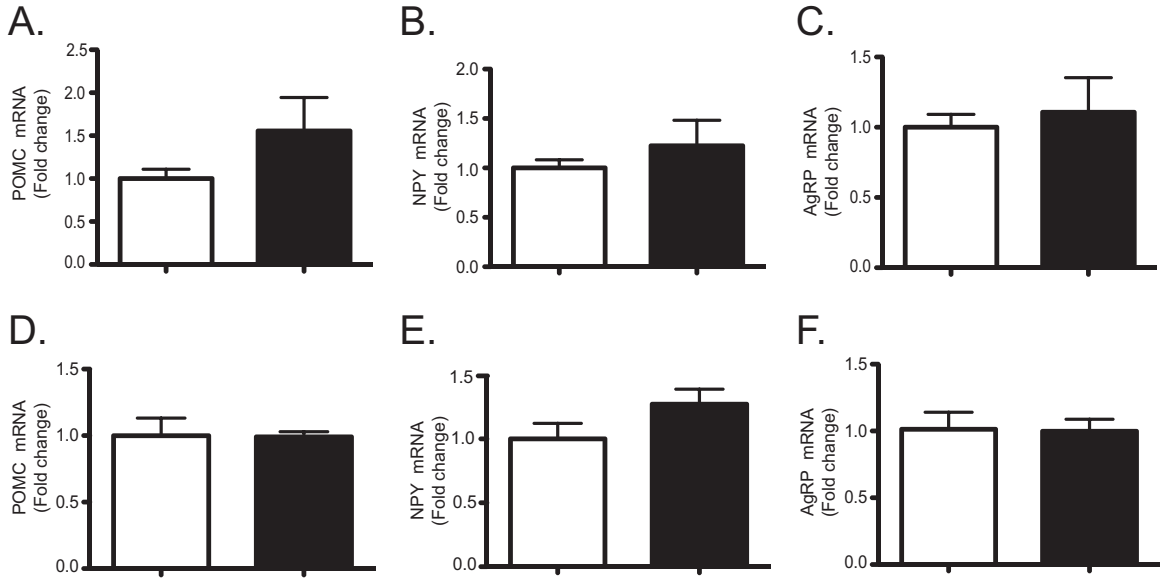

FIG 10 Effects on hypothalamic neuropeptide expression in MKP1-LKO mice. RNA was isolated from the brain of chow-fed (A to C) and HFD-fed (D to F) *Mkp-1*$^{fl/fl}$ and MKP1-LKO mice, and the expression of POMC, NPY, and AgRP was analyzed by quantitative PCR ($n = 5$ per genotype). Data are represented as means ± SEM. Open bars, *Mkp-1*$^{fl/fl}$ mice; filled bars, MKP1-LKO mice.

to promote energy expenditure. The liver is one of the major sources of the circulating hormone fibroblast growth factor 21 (FGF21), which promotes energy expenditure, insulin sensitivity, fatty acid oxidation, and weight loss (30). Since FGF21 is a potent starvation-sensitive hepatokine, we determined its expression in fasted and refed MKP1-LKO mice. These results demonstrated that whereas FGF21 expression was robustly upregulated in fasted wild-type mice, MKP1-LKO mice failed to upregulate FGF21 when fasted (Fig. 11A). The hepatic expression levels of FGF15/19 and FGF23 were not detectable in either *Mkp-1*$^{fl/fl}$ or MKP1-LKO mice. The circulating expression levels of FGF21 in MKP1-LKO mice were significantly reduced in chow-fed but not HFD-fed MKP1-LKO mice compared with those in *Mkp-1*$^{fl/fl}$ mice (Fig. 11B). We found no significant differences in components of ketogenesis, such as β-hydroxybutyrate in MKP1-LKO mice fed a chow diet (Fig. 11C) or mitochondrial 3-hydroxy-3-methylglutaryl-CoA synthase (HMGCS2) expression, either under fasted or fed conditions (Fig. 11D).

Next, we determined whether MKP-1 regulates FGF21 in a cell-autonomous manner. Primary hepatocytes were isolated from MKP1-LKO and *Mkp-1*$^{fl/fl}$ mice and transiently transfected with the promoter of FGF21 fused to luciferase (31). Basal levels of FGF21 promoter activity were significantly lower in hepatocytes from MKP1-LKO mice than in those from *Mkp-1*$^{fl/fl}$ controls (Fig. 11E). These results demonstrate that hepatic MKP-1 is required for the transcriptional expression of FGF21 in hepatocytes and implies that MAPK activity suppresses FGF21 transcriptional responsiveness. To identify which MAPK suppresses FGF21 expression, hepatocytes from *Mkp-1*$^{fl/fl}$ mice were transiently transfected with the FGF21 luciferase reporter and were preincubated with MAPK inhibitors of p38 MAPK (SB203580), JNK (SP60015), and MEK (U0126) prior to stimulation with glucagon to promote both the expression of MKP-1 and FGF21 (32, 33). We found that inhibition of p38 MAPK significantly relieved suppression of FGF21 promoter activity (Fig. 11F), whereas pharmacological inhibition of JNK had a marginal effect and inhibition of MEK further suppressed FGF21-mediated reporter activity (Fig. 11F). To support the pharmacological interpretation suggesting a predominant role for p38 MAPK in the suppression of FGF21 expression, we employed gain-of and loss-of-function approaches using the upstream activators of p38 MAPK and JNK, MKK6, and MKK4, respectively. Since no discernible differences in ERK1/2 activities were found in the livers of MKP1-LKO mice (Fig. 2), we focused on p38 MAPK and JNK for these analyses. When HepG2 cells were transfected with an activating mutant of MKK6 to activate constitutively p38 MAPK, FGF21 reporter activity was suppressed (Fig. 11G). In contrast, a dominant negative mutant of MKK6 relieved this inhibition (Fig. 11G). Given the importance of JNK in hepatic metabolism (11), we were surprised that neither gain- nor loss-of-function MKK4 mutants affected FGF21 reporter activity (Fig. 11G). As a control, the expected increase and decrease in levels of p38 MAPK and JNK1/2 phosphorylation were observed with the respective constitutively activated and dominant negative mutants of MKK6 and MKK4 (Fig. 11G). Together, these data suggest that MKP-1 is required for the expression of FGF21 in hepatocytes in a p38 MAPK-dependent manner.

Hepatic MKP-1 regulates skeletal muscle metabolism. We next sought to establish whether peripheral tissues exhibit impaired metabolic flux that would be consistent with the reduced levels of circulating IL-6 and FGF21. Supporting evidence that loss of hepatic MKP-1 could affect skeletal muscle metabolism was first provided by the observation that MKP1-LKO mice expressed significantly reduced PGC-1α mRNA in skeletal muscle under both chow diet and HFD conditions compared with that for *Mkp-1*$^{fl/fl}$ controls (Fig. 12A). We next measured mitochondrial respiration in permeabilized soleus muscle fibers isolated from chow- and HFD-fed MKP1-LKO and *Mkp-1*$^{fl/fl}$ mice. Under both chow- and HFD-fed conditions, the respiratory control ratio significantly decreased in MKP1-LKO mice compared with that in *Mkp-1*$^{fl/fl}$ controls (Fig. 12B). Collectively, these data demonstrate

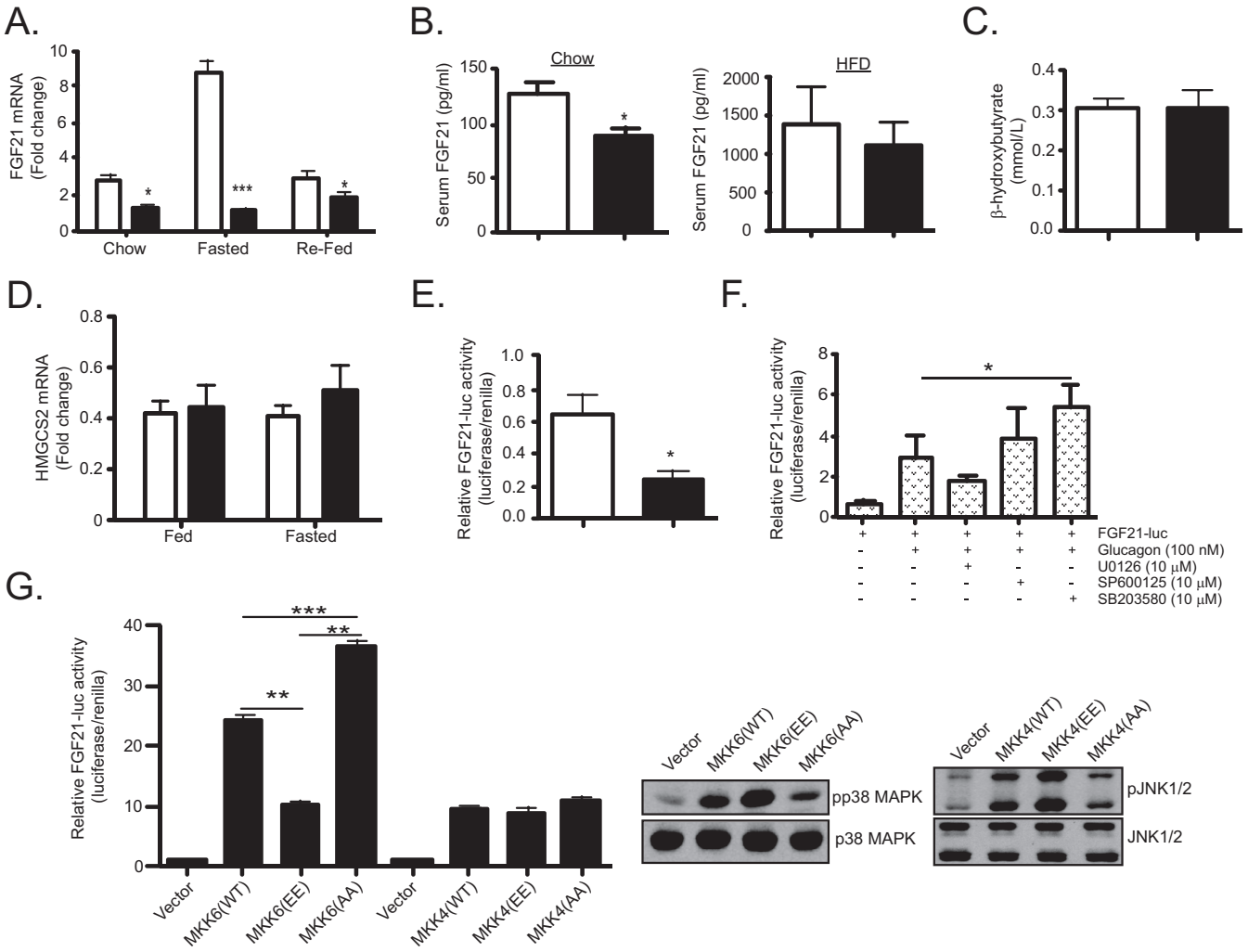

FIG 11 Hepatic MKP-1 is required for FGF21 expression and skeletal muscle metabolism. (A) Hepatic FGF21 mRNA expression in chow-fed, fasted, and refed mice ($n = 8$ per genotype). (B) Serum FGF21 levels ($n = 8$ per genotype). (C) Hepatic β-hyroxybutyrate expression in chow-fed mice ($n = 5$ per genotype). (D) HMGCS2 mRNA expression in fed and fasted animals ($n = 10$ per genotype). (E) Relative luciferase activity in hepatocytes derived from *Mkp-1*$^{fl/fl}$ and MKP1-LKO mice transfected with the FGF21 luciferase promoter ($n = 3$ or 4 independent experiments). (F) Relative luciferase activity in hepatocytes derived from *Mkp-1*$^{fl/fl}$ mice transfected with FGF21 luciferase promoter for 48 h, following incubation with vehicle or MAPK inhibitors for 1 h prior to stimulation with glucagon for 6 h ($n = 3$ or 4). (G) HepG2 cells were cotransfected with the FGF21 luciferase promoter and either the wild type or constitutively active mutants of the upstream activators of p38 MAPK (MKK6EE) and JNK (MKK4EE) or dominant negative mutants of p38 MAPK [MKK6(AA)] and JNK [MKK4(AA)]. HepG2 cells were lysed and immunoblotted for phospho-p38 MAPK and phospho-JNK ($n = 3$ or 4). Data are represented as means ± SEM; *, $P < 0.05$; **, $P < 0.01$; ***, $P < 0.0001$ (as determined by Student's *t* test). Open bars, *Mkp-1*$^{fl/fl}$ mice; filled bars, MKP1-LKO mice.

that hepatic deletion of MKP-1 results in reduced circulating IL-6 and FGF21 levels and this is associated with impaired skeletal muscle oxidative capacity and susceptibility to diet-induced obesity.

DISCUSSION

The tissue-specific contributions of MKP-1 in physiology are unknown. Previously, whole-body deletion of MKP-1 was found to result in resistance to diet-induced obesity and protection from the acquisition of hepatosteatosis in models of diet-induced and genetic obesity (15–17). Our goal in this study was to specifically examine the hepatic function of MKP-1 in mice. In order to achieve this, we generated liver-specific-MKP-1-deficient mice. The results of this study revealed that hepatic MKP-1 serves as a master regulator of MAPK-dependent pathways that selectively target, in a mutually exclusive manner, gluconeogenic and lipogenic processes. Moreover, our results reveal that hepatic MKP-1 plays a role in the control of endocrine effects that stem from the regulation of both IL-6 and FGF21 (Fig. 12C).

Our studies demonstrate an essential role for MKP-1 in gluconeogenesis through the control of MAPK-mediated pathways that participate in the regulation of STAT-3 through control of both tyrosine and serine STAT-3 phosphorylation. In addition, CREB-mediated gluconeogenic gene activation (23) is negatively regulated by hepatic MKP-1 through a p38 MAPK-dependent pathway. The observation that STAT-3 signaling was impaired by loss of hepatic MKP-1 was ascribed to the reduced circulating IL-6 levels. These results uncover the surprising relationship between hepatic MKP-1 and the expression of IL-6. Although IL-6 acts on the liver to suppress gluconeogenesis, this cytokine is secreted primarily from the hypothalamus, adipose tissue, and skeletal mus-

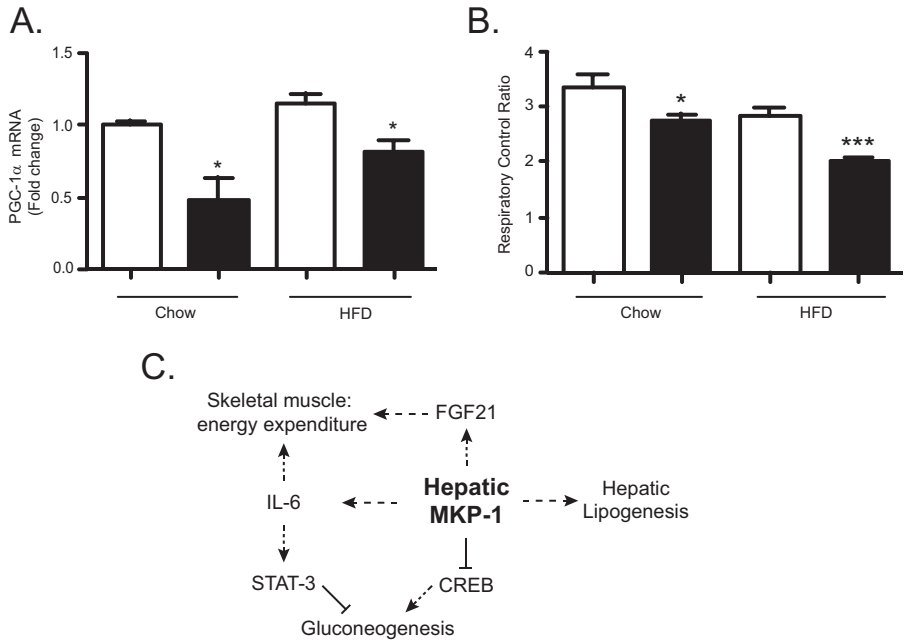

FIG 12 Hepatic MKP-1 regulates skeletal muscle mitochondrial respiration. (A) mRNA expression of PGC-1α from skeletal muscle of chow and HFD-fed *Mkp-1*$^{fl/fl}$ and MKP1-LKO mice ($n = 5$ per genotype). (B) Mitochondrial respiratory function in skeletal muscle of chow ($n = 6$ per genotype) and HFD-fed ($n = 8$ per genotype) *Mkp-1*$^{fl/fl}$ and MKP1-LKO mice. Data are represented as means ± SEM; *, $P < 0.05$; ***, $P < 0.0001$ (as determined by Student's *t* test). Open bars, *Mkp-1*$^{fl/fl}$ mice; filled bars, MKP1-LKO mice. (C) Integrative mode of metabolic regulation by hepatic MKP-1. In obesity, overexpressed hepatic MKP-1 selectively drives lipogenesis, thereby contributing to the development of hepatosteatosis.

cle. Therefore, hepatic MKP-1 likely influences IL-6 expression by acting on an endocrine pathway that indirectly controls IL-6 expression in one or more of these tissues. The exact nature of this integration between the role of the hepatic MKP-1 and other tissues remains to be resolved.

The selectivity of hepatic MKP-1-mediated effects on gluconeogenesis and lipogenesis is supported by the observation that obese mice overexpressing hepatic MKP-1 exhibit fasting hyperglycemia in the background of persistent lipogenesis, a hallmark of the type 2 diabetic state. Additionally, neither lipotoxicity nor endoplasmic reticulum stress was evident in MKP1-LKO mice under chow-fed conditions where hepatic insulin resistance was observed, suggesting that loss of hepatic MKP-1 perturbs hepatic metabolic homeostasis discretely. Thus, MKP-1 negatively engages MAPK-dependent pathways in the liver under basal conditions to control gluconeogenesis and lipogenesis (Fig. 12C). However, when MKP-1 is overexpressed in pathophysiological situations, such as in obesity, these pathways become uncoupled. Interestingly, it has been reported that hepatic p38 MAPK activity decreases in HFD-fed mice (34), raising the possibility that MKP-1 overexpression contributes to the dephosphorylation of p38 MAPK and exacerbates the loss of glucose homeostasis while promoting lipogenesis.

MKP-1 dephosphorylates and inactivates hepatic JNK1/2. Consistent with this, liver-specific deletion of JNK1 promotes hepatosteatosis (11). However, hepatic JNK1-deficient mice exhibit hepatic insulin resistance, while MKP1-LKO mice show enhanced hepatic JNK1/2 activity that correlates with a dissociation of hepatic steatosis from insulin resistance. These observations provide additional support for the notion that MKP-1 engages selectively with distinct MAPK-directed metabolic pathways in the liver. Indeed, it is noteworthy that MKP1-LKO mice reciprocally phenocopy liver-specific CREB disruption, since CREB mutant mice display increased hepatosteatosis and lipogenesis but decreased gluconeogenesis (22, 23). Thus, MKP-1 likely lies upstream of CREB in the liver, and by inference, nuclearly localized p38 MAPK dephosphorylation contributes to the balance of metabolic flux between glucose and lipid metabolism. In addition to MKP-1, it has also been suggested that other MKPs participate in the regulation of gluconeogenesis. MKP-3, which dephosphorylates primarily ERK1/2 (35), was shown to also dephosphorylate a noncanonical MKP motif on the forkhead box O1 (FOXO1) (36). When dephosphorylated by MKP-3, FOXO1 translocates to the nucleus, where it engages gluconeogenic gene expression. Since ERK1/2 and p38 MAPK can also phosphorylate FOXO1 (37), it is formally possible that MKP-3 dephosphorylates ERK1/2, leading to reduced FOXO1 phosphorylation and nuclear translocation. It has been shown that JNK can also promote the phosphorylation of some (38) but not all FOXO isoforms (37). However, whether JNK/FOXO signaling in the liver plays a role in the control of gluconeogenesis, in addition to its purported effects on longevity and stress responsiveness, remains unclear (39). Constitutive activation of FOXO1 promotes gluconeogenesis and causes hepatosteatosis (40). This phenotype is distinct from that seen in MKP1-LKO mice, which are protected against hepatosteatosis. These observations suggest that hepatic MKP-1/JNK/FOXO signaling is less likely to make a significant contribution to the manifestation of the MKP1-LKO phenotype.

The susceptibility of MKP1-LKO mice to developing increased adiposity on chow and following high-fat feeding was surprising in light of the observation that whole-body-MKP-1-deficient mice are resistant to diet-induced obesity (15, 16). This is likely attrib-

utable to reduced whole-body energy expenditure, since neither differences in feeding nor in locomotor activity were observed between MKP1-LKO and control mice. We identified FGF21 as a candidate that may account, at least in part, for the reduced energy expenditure, since FGF21 is a known metabolic endocrine hormone expressed predominately in the liver (41). PGC-1α has been shown to negatively regulate FGF21 expression (42), and MKP-1 negatively regulates PGC-1α function in a p38 MAPK-dependent manner (16). Therefore, our data imply a link between MKP-1/p38 MAPK and the negative regulation of FGF21 by PGC-1α, since we show that p38 MAPK mediates the inhibitory effect on FGF21 expression.

Obese patients that are type 2 diabetic or who present with nonalcoholic steatosis have elevated serum FGF21 levels (41); this is consistent with our observation that hepatic MKP-1 is overexpressed in obesity. FGF21 stimulates the expression of PGC-1α to drive mitochondrial oxidation in white adipose tissue (43), and here we found decreased skeletal muscle PGC-1α expression in MKP1-LKO mice, which provides a mechanism for the impaired skeletal muscle mitochondrial respiration (Fig. 12C). It is also conceivable that FGF21 acts indirectly on skeletal muscle through a local adiponectin/p38 MAPK/MKP-1 pathway (44, 45) to contribute to mitochondrial function. Recently, it has been suggested that FGF21 is negatively regulated by JNK through a PPARα-dependent pathway (46). It is not clear why at this juncture; we do not appear to find evidence for a role of JNK in the control of FGF21. Actions of JNK indirectly affecting the status of p38 MAPK-mediated signaling remain one possible explanation. It is also noteworthy that the reduced level of IL-6, which we propose contributes to the impairment of gluconeogenesis (Fig. 12C), is also likely to indirectly influence metabolic homeostasis. Given the important role of inflammation in metabolic homeostasis (27), the relative contributions of both IL-6 and FGF-21 to the overall metabolic phenotype of MKP1-LKO mice are likely to be quite complex. In summary, we have revealed an unanticipated selectivity of hepatic MKP-1 in metabolic disease and define a pathway in which hepatic MKP-1 is critical for liver metabolism and maintenance of peripheral tissue energy homeostasis. This study highlights the complexity of nuclearly localized MAPK dephosphorylation by MKP-1 in the liver.

ACKNOWLEDGMENTS

This work was supported by NIH grant R01 DK57765 to A.M.B., a Browne-Cox Fellowship awarded to A.L., and Yale Liver Center grant P30 DK34989. G.I.S. is supported by R01 DK40936, R24 DK085638, P30 DK45735, and U24 DK059635 (Yale MMPC) and the Howard Hughes Medical Institute.

REFERENCES

1. **Hosseinpoor AR, Stewart Williams JA, Itani L, Chatterji S.** 2012. Socioeconomic inequality in domains of health: results from the World Health Surveys. BMC Public Health **12:**198. http://dx.doi.org/10.1186/1471-2458-12-198.
2. **Cohen JC, Horton JD, Hobbs HH.** 2011. Human fatty liver disease: old questions and new insights. Science **332:**1519–1523. http://dx.doi.org/10.1126/science.1204265.
3. **Sun Z, Lazar MA.** 2013. Dissociating fatty liver and diabetes. Trends Endocrinol Metab **24:**4–12. http://dx.doi.org/10.1016/j.tem.2012.09.005.
4. **Samuel VT, Shulman GI.** 2012. Mechanisms for insulin resistance: common threads and missing links. Cell **148:**852–871. http://dx.doi.org/10.1016/j.cell.2012.02.017.
5. **Tanti JF, Jager J.** 2009. Cellular mechanisms of insulin resistance: role of stress-regulated serine kinases and insulin receptor substrates (IRS) serine phosphorylation. Curr Opin Pharmacol **9:**753–762. http://dx.doi.org/10.1016/j.coph.2009.07.004.
6. **Leavens KF, Birnbaum MJ.** 2011. Insulin signaling to hepatic lipid metabolism in health and disease. Crit Rev Biochem Mol Biol **46:**200–215. http://dx.doi.org/10.3109/10409238.2011.562481.
7. **Hirosumi J, Tuncman G, Chang L, Gorgun CZ, Uysal KT, Maeda K, Karin M, Hotamisligil GS.** 2002. A central role for JNK in obesity and insulin resistance. Nature **420:**333–336. http://dx.doi.org/10.1038/nature01137.
8. **Jager J, Corcelle V, Gremeaux T, Laurent K, Waget A, Pages G, Binetruy B, Le Marchand-Brustel Y, Burcelin R, Bost F, Tanti JF.** 2011. Deficiency in the extracellular signal-regulated kinase 1 (ERK1) protects leptin-deficient mice from insulin resistance without affecting obesity. Diabetologia **54:**180–189. http://dx.doi.org/10.1007/s00125-010-1944-0.
9. **Cao W, Collins QF, Becker TC, Robidoux J, Lupo EG, Jr, Xiong Y, Daniel KW, Floering L, Collins S.** 2005. p38 Mitogen-activated protein kinase plays a stimulatory role in hepatic gluconeogenesis. J Biol Chem **280:**42731–42737. http://dx.doi.org/10.1074/jbc.M506223200.
10. **Sabio G, Davis RJ.** 2010. cJun NH2-terminal kinase 1 (JNK1): roles in metabolic regulation of insulin resistance. Trends Biochem Sci **35:**490–496. http://dx.doi.org/10.1016/j.tibs.2010.04.004.
11. **Sabio G, Cavanagh-Kyros J, Ko HJ, Jung DY, Gray S, Jun JY, Barrett T, Mora A, Kim JK, Davis RJ.** 2009. Prevention of steatosis by hepatic JNK1. Cell Metab **10:**491–498. http://dx.doi.org/10.1016/j.cmet.2009.09.007.
12. **Collins QF, Xiong Y, Lupo EG, Jr, Liu HY, Cao W.** 2006. p38 Mitogen-activated protein kinase mediates free fatty acid-induced gluconeogenesis in hepatocytes. J Biol Chem **281:**24336–24344. http://dx.doi.org/10.1074/jbc.M602177200.
13. **Lawan A, Shi H, Gatzke F, Bennett AM.** 2013. Diversity and specificity of the mitogen-activated protein kinase phosphatase-1 functions. Cell Mol Life Sci **70:**223–237. http://dx.doi.org/10.1007/s00018-012-1041-2.
14. **Lawan A, Bennett AM.** 2013. MAP kinase phosphatases emerge as new players in metabolic regulation, p 221. *In* Bence KK (ed), Protein tyrosine phosphatase control of metabolism. Springer, New York, NY.
15. **Wu JJ, Roth RJ, Anderson EJ, Hong E-G, Lee M-K, Choi CS, Neufer PD, Shulman GI, Kim JK, Bennett AM.** 2006. Mice lacking MAP kinase phosphatase-1 have enhanced MAP kinase activity and resistance to diet-induced obesity. Cell Metab **4:**61–73. http://dx.doi.org/10.1016/j.cmet.2006.05.010.
16. **Roth RJ, Le AM, Zhang L, Kahn M, Samuel VT, Shulman GI, Bennett AM.** 2009. MAPK phosphatase-1 facilitates the loss of oxidative myofibers associated with obesity in mice. J Clin Invest **119:**3817–3829. http://dx.doi.org/10.1172/JCI39054.
17. **Flach RJ, Qin H, Zhang L, Bennett AM.** 2011. Loss of mitogen-activated protein kinase phosphatase-1 protects from hepatic steatosis by repression of cell death-inducing DNA fragmentation factor A (DFFA)-like effector C (CIDEC)/fat-specific protein 27. J Biol Chem **286:**22195–22202. http://dx.doi.org/10.1074/jbc.M110.210237.
18. **Lee J, Ozcan U.** 2014. Unfolded protein response signaling and metabolic diseases. J Biol Chem **289:**1203–1211. http://dx.doi.org/10.1074/jbc.R113.534743.
19. **Qiao L, MacDougald OA, Shao J.** 2006. CCAAT/enhancer-binding protein alpha mediates induction of hepatic phosphoenolpyruvate carboxykinase by p38 mitogen-activated protein kinase. J Biol Chem **281:**24390–24397. http://dx.doi.org/10.1074/jbc.M603038200.
20. **Roden M, Bernroider E.** 2003. Hepatic glucose metabolism in humans—its role in health and disease. Best Pract Res Clin Endocrinol Metab **17:**365–383. http://dx.doi.org/10.1016/S1521-690X(03)00031-9.
21. **Yoon JC, Puigserver P, Chen G, Donovan J, Wu Z, Rhee J, Adelmant G, Stafford J, Kahn CR, Granner DK, Newgard CB, Spiegelman BM.** 2001. Control of hepatic gluconeogenesis through the transcriptional coactivator PGC-1. Nature **413:**131–138. http://dx.doi.org/10.1038/35093050.
22. **Herzig S, Hedrick S, Morantte I, Koo SH, Galimi F, Montminy M.** 2003. CREB controls hepatic lipid metabolism through nuclear hormone receptor PPAR-gamma. Nature **426:**190–193. http://dx.doi.org/10.1038/nature02110.
23. **Herzig S, Long F, Jhala US, Hedrick S, Quinn R, Bauer A, Rudolph D, Schutz G, Yoon C, Puigserver P, Spiegelman B, Montminy M.** 2001. CREB regulates hepatic gluconeogenesis through the coactivator PGC-1. Nature **413:**179–183. http://dx.doi.org/10.1038/35093131.
24. **Wu JJ, Bennett AM.** 2005. Essential role for mitogen-activated protein (MAP) kinase phosphatase-1 in stress-responsive MAP kinase and cell

survival signaling. J Biol Chem **280:**16461–16466. http://dx.doi.org/10.1074/jbc.M501762200.

25. **Inoue H, Ogawa W, Ozaki M, Haga S, Matsumoto M, Furukawa K, Hashimoto N, Kido Y, Mori T, Sakaue H, Teshigawara K, Jin S, Iguchi H, Hiramatsu R, LeRoith D, Takeda K, Akira S, Kasuga M.** 2004. Role of STAT-3 in regulation of hepatic gluconeogenic genes and carbohydrate metabolism in vivo. Nat Med **10:**168–174. http://dx.doi.org/10.1038/nm980.
26. **Wen Z, Zhong Z, Darnell JE, Jr.** 1995. Maximal activation of transcription by Stat1 and Stat3 requires both tyrosine and serine phosphorylation. Cell **82:**241–250. http://dx.doi.org/10.1016/0092-8674(95)90311-9.
27. **Hassan W, Ding L, Gao RY, Liu J, Shang J.** 2014. Interleukin-6 signal transduction and its role in hepatic lipid metabolic disorders. Cytokine **66:**133–142. http://dx.doi.org/10.1016/j.cyto.2013.12.017.
28. **Wallenius V, Wallenius K, Ahren B, Rudling M, Carlsten H, Dickson SL, Ohlsson C, Jansson JO.** 2002. Interleukin-6-deficient mice develop mature-onset obesity. Nat Med **8:**75–79. http://dx.doi.org/10.1038/nm0102-75.
29. **Coskun T, Bina HA, Schneider MA, Dunbar JD, Hu CC, Chen Y, Moller DE, Kharitonenkov A.** 2008. Fibroblast growth factor 21 corrects obesity in mice. Endocrinology **149:**6018–6027. http://dx.doi.org/10.1210/en.2008-0816.
30. **Cicione C, Degirolamo C, Moschetta A.** 2012. Emerging role of fibroblast growth factors 15/19 and 21 as metabolic integrators in the liver. Hepatology **56:**2404–2411. http://dx.doi.org/10.1002/hep.25929.
31. **Inagaki T, Dutchak P, Zhao G, Ding X, Gautron L, Parameswara V, Li Y, Goetz R, Mohammadi M, Esser V, Elmquist JK, Gerard RD, Burgess SC, Hammer RE, Mangelsdorf DJ, Kliewer SA.** 2007. Endocrine regulation of the fasting response by PPARalpha-mediated induction of fibroblast growth factor 21. Cell Metab **5:**415–425. http://dx.doi.org/10.1016/j.cmet.2007.05.003.
32. **Habegger KM, Stemmer K, Cheng C, Muller TD, Heppner KM, Ottaway N, Holland J, Hembree JL, Smiley D, Gelfanov V, Krishna R, Arafat AM, Konkar A, Belli S, Kapps M, Woods SC, Hofmann SM, D'Alessio D, Pfluger PT, Perez-Tilve D, Seeley RJ, Konishi M, Itoh N, Kharitonenkov A, Spranger J, Dimarchi RD, Tschop MH.** 2013. Fibroblast growth factor 21 mediates specific glucagon actions. Diabetes **62:**1453–1463. http://dx.doi.org/10.2337/db12-1116.
33. **Schliess F, Kurz AK, Haussinger D.** 2000. Glucagon-induced expression of the MAP kinase phosphatase MKP-1 in rat hepatocytes. Gastroenterology **118:**929–936. http://dx.doi.org/10.1016/S0016-5085(00)70179-X.
34. **Lee J, Sun C, Zhou Y, Lee J, Gokalp D, Herrema H, Park SW, Davis RJ, Ozcan U.** 2011. p38 MAPK-mediated regulation of Xbp1s is crucial for glucose homeostasis. Nat Med **17:**1251–1260. http://dx.doi.org/10.1038/nm.2449.
35. **Camps M, Nichols A, Arkinstall S.** 2000. Dual specificity phosphatases: a gene family for control of MAP kinase function. FASEB J **14:**6–16.
36. **Wu Z, Jiao P, Huang X, Feng B, Feng Y, Yang S, Hwang P, Du J, Nie Y, Xiao G, Xu H.** 2010. MAPK phosphatase-3 promotes hepatic gluconeogenesis through dephosphorylation of forkhead box O1 in mice. J Clin Invest **120:**3901–3911. http://dx.doi.org/10.1172/JCI43250.
37. **Asada S, Daitoku H, Matsuzaki H, Saito T, Sudo T, Mukai H, Iwashita S, Kako K, Kishi T, Kasuya Y, Fukamizu A.** 2007. Mitogen-activated protein kinases, Erk and p38, phosphorylate and regulate Foxo1. Cell Signal **19:**519–527. http://dx.doi.org/10.1016/j.cellsig.2006.08.015.
38. **Essers MA, Weijzen S, de Vries-Smits AM, Saarloos I, de Ruiter ND, Bos JL, Burgering BM.** 2004. FOXO transcription factor activation by oxidative stress mediated by the small GTPase Ral and JNK. EMBO J **23:**4802–4812. http://dx.doi.org/10.1038/sj.emboj.7600476.
39. **Matsumoto M, Accili D.** 2005. All roads lead to FoxO. Cell Metab **1:**215–216. http://dx.doi.org/10.1016/j.cmet.2005.03.008.
40. **Matsumoto M, Han S, Kitamura T, Accili D.** 2006. Dual role of transcription factor FoxO1 in controlling hepatic insulin sensitivity and lipid metabolism. J Clin Invest **116:**2464–2472. http://dx.doi.org/10.1172/JCI27047.
41. **Potthoff MJ, Kliewer SA, Mangelsdorf DJ.** 2012. Endocrine fibroblast growth factors 15/19 and 21: from feast to famine. Genes Dev **26:**312–324. http://dx.doi.org/10.1101/gad.184788.111.
42. **Estall JL, Ruas JL, Choi CS, Laznik D, Badman M, Maratos-Flier E, Shulman GI, Spiegelman BM.** 2009. PGC-1alpha negatively regulates hepatic FGF21 expression by modulating the heme/Rev-Erb(alpha) axis. Proc Natl Acad Sci U S A **106:**22510–22515. http://dx.doi.org/10.1073/pnas.0912533106.
43. **Potthoff MJ, Inagaki T, Satapati S, Ding X, He T, Goetz R, Mohammadi M, Finck BN, Mangelsdorf DJ, Kliewer SA, Burgess SC.** 2009. FGF21 induces PGC-1alpha and regulates carbohydrate and fatty acid metabolism during the adaptive starvation response. Proc Natl Acad Sci U S A **106:**10853–10858. http://dx.doi.org/10.1073/pnas.0904187106.
44. **Lin Z, Tian H, Lam KS, Lin S, Hoo RC, Konishi M, Itoh N, Wang Y, Bornstein SR, Xu A, Li X.** 2013. Adiponectin mediates the metabolic effects of FGF21 on glucose homeostasis and insulin sensitivity in mice. Cell Metab **17:**779–789. http://dx.doi.org/10.1016/j.cmet.2013.04.005.
45. **Qiao L, Kinney B, Yoo HS, Lee B, Schaack J, Shao J.** 2012. Adiponectin increases skeletal muscle mitochondrial biogenesis by suppressing mitogen-activated protein kinase phosphatase-1. Diabetes **61:**1463–1470. http://dx.doi.org/10.2337/db11-1475.
46. **Vernia S, Cavanagh-Kyros J, Garcia-Haro L, Sabio G, Barrett T, Jung DY, Kim JK, Xu J, Shulha HP, Garber M, Gao G, Davis RJ.** 2014. The PPARalpha-FGF21 hormone axis contributes to metabolic regulation by the hepatic JNK signaling pathway. Cell Metab **20:**512–525. http://dx.doi.org/10.1016/j.cmet.2014.06.010.